

TOPICAL REVIEW

Thermal interface materials with graphene fillers: review of the state of the art and outlook for future applications

To cite this article: Jacob S Lewis *et al* 2021 *Nanotechnology* **32** 142003

View the [article online](#) for updates and enhancements.

The 17th International Symposium on Solid Oxide Fuel Cells (SOFC-XVII)
DIGITAL MEETING • July 18-23, 2021

EXTENDED Abstract Submission Deadline: February 19, 2021



SUBMIT NOW →

Topical Review

Thermal interface materials with graphene fillers: review of the state of the art and outlook for future applications

Jacob S Lewis^{1,2} , Timothy Perrier^{1,3} , Zahra Barani^{1,3},
Fariborz Kargar^{1,3}  and Alexander A Balandin^{1,2,3} 

¹ Phonon Optimized Engineered Materials (POEM) Center, University of California, Riverside, CA 92521, United States of America

² Materials Science and Engineering Program, Bourns College of Engineering, University of California, Riverside, CA 92521, United States of America

³ Department of Electrical and Computer Engineering, Bourns College of Engineering, University of California, Riverside, CA 92521, United States of America

E-mail: jlewi014@ucr.edu and balandin@ece.ucr.edu

Received 26 July 2020, revised 6 September 2020

Accepted for publication 13 October 2020

Published 13 January 2021



CrossMark

Abstract

We review the current state-of-the-art graphene-enhanced thermal interface materials for the management of heat in the next generation of electronics. Increased integration densities, speed and power of electronic and optoelectronic devices require thermal interface materials with substantially higher thermal conductivity, improved reliability, and lower cost. Graphene has emerged as a promising filler material that can meet the demands of future high-speed and high-powered electronics. This review describes the use of graphene as a filler in curing and non-curing polymer matrices. Special attention is given to strategies for achieving the thermal percolation threshold with its corresponding characteristic increase in the overall thermal conductivity. Many applications require high thermal conductivity of composites, while simultaneously preserving electrical insulation. A hybrid filler approach, using graphene and boron nitride, is presented as a possible technology providing for the independent control of electrical and thermal conduction. The reliability and lifespan performance of thermal interface materials is an important consideration towards the determination of appropriate practical applications. The present review addresses these issues in detail, demonstrating the promise of graphene-enhanced thermal interface materials compared to alternative technologies.

Keywords: graphene, thermal management, thermal percolation, synergistic enhancement, polymer composites, thermal conductivity, boron nitride

(Some figures may appear in colour only in the online journal)

1. Introduction

The extraordinary increase in transistor density in semiconductor products has revolutionized our society and introduced new challenges towards its continued progress [1]. Although the decreasing feature size that enables ever-increasing densification and computational power has

typically brought with it per-transistor energy efficiency enhancements, this does not make up for the overall waste heat production that results from having more switches in total in the same area [2, 3]. This has led to a general trend for very large-scale integration (VLSI) chips to increase in thermal design power at every generation, with notable deviations from this trend usually coming in the form of vast

architectural improvements or splitting the die into multiple logical cores. The increase in dissipated heat is problematic for VLSI semiconductor chips because their functionality can unacceptably alter at high temperatures, due for instance to hot carrier degradation and bias temperature instability [4–6]. Now that devices are manufactured in the sub-10-nanometer process, it is becoming more difficult to manage waste heat production due to ever more important factors such as leakage current and Joule heating in interconnect circuit elements of decreasing cross-sectional area. Each of these serves to make improved thermal dissipative solutions increasingly essential. In parallel, the growing fields of light-emitting diode (LED) lighting and solar energy along with the continuation of aerospace products all require similar and improved heat dissipation solutions [7–14].

The scale of the waste heat problem in semiconductors is often lost in the numbers, even among researchers. The *average* power density of some modern silicon VLSI chips can reach as high as 1/100 of the power density at the top of the Sun's photosphere, which is approximately 6300 W cm^{-2} . However, when one takes a more detailed look at a modern VLSI chip one will find local spots in which the heat density is substantially higher than the average [15]. VLSI chips operate at such reasonable temperatures despite their staggering heat production, solely because of their accompanying engineered thermal dissipation solutions.

The most common technique to remove heat from VLSI chips and other semiconductor circuits is to bring metals—termed heat sinks—in contact with the chip so the heat may diffuse into this additional component. The heat absorbed by the sink is then more effectively dissipated to the environment, with a presumably infinite thermal reservoir capacity, due to its large surface area. Often the heat sink employs heat pipes—sealed tubes often with a phase-changing fluid inside of it—that add convection and heat of vaporization at each end as mechanisms of heat transfer along with the conduction of the metallic pipe material [16, 17]. The heat sink class of thermal dissipation solutions are cheap, reliable, small, and ubiquitous.

All thermal dissipation solutions in which a solid heat-producing device is placed in contact with a solid heat sink suffer from physical junction thermal interface resistance. Between any two solid, non-compliant materials, the total percentage of surface area making contact can be quite low, with a strong dependence on factors such as microscopic scale surface roughness, material plasticity, and mounting pressure [18–20]. A low proportion of direct surface contact at a physical junction inevitably means that gaps are filled with air, which has very poor heat transfer characteristics relative to the metals on each side of the junction. The heat flow from source to drain is analogous to and often thought of as an electrical circuit, in which the metal components of the dissipative solution are low-resistance wires with the junction thought of as a resistor. The thermal resistance between two physical junctions is often termed contact resistance, R_C . The thermal resistance of a junction is substantially reduced with the use of an interstitial material called a thermal interface

material (TIM) [21]. The resistance of the junction is then:

$$R_{TIM} = \frac{BLT}{K} + R_{C1} + R_{C2}, \quad (1)$$

where BLT is the bondline thickness, K is the thermal conductivity (TC) of the TIM itself, and R_{C1} and R_{C2} are the contact resistances of each junction surface with the TIM [22–24]. For an appropriate TIM, $R_{TIM} < R_C$. It is clear from equation (1) that for increasing BLT the TC becomes an ever more important factor in R_{TIM} . Figure 1(a) shows a schematic highlighting the benefit of TIMs in an exaggeratedly imperfect junction in which a greater portion of the junction's surface area is used for heat dissipation with TIMs applied versus without.

TIM materials are often composed of metal solders, mechanically compliant pads, and polymers typically composed with filler materials [26]. Each type of TIM has its own strengths and weaknesses. Metal TIMs to date have achieved the lowest thermal interface resistance at initial application. There can be variations in the precise functionality of this class of TIM, but they typically are introduced to the junction as a hot liquid and are frozen to a solid between the two surfaces. However, they can exist in either a permanently liquid state or change between the two. Metal TIMs can achieve a TC over 86 W/mK —that of indium—and an interfacial resistance of $0.005 \text{ K cm}^2/\text{W}$ [27–30]. The thermal transport in metallic TIMs is predominantly contributed to by their substantial population of free electrons, as in all metals, carrying heat mostly freely within the material's spatial confines. Although these TIMs remain, at the time of this article, as the best-performing at application, they are marred by reliability problems and are more expensive than alternatives. Due to the reliability concerns of metallic TIMs, it is a very active area of research for these materials [27, 31–36]. Metal TIM suffers from poor lifespan performance because it is typically frozen between two surfaces of different coefficients of thermal expansion to each other and itself. As the temperature of the junction is inevitably varied, disadvantageous thermomechanical stress is inadvertently applied to the TIM, which eventually cracks it, leading to substantially reduced performance. That same thermal expansion mechanism can result in pushing fluid TIMs out of the junction in a process called 'pumping out.' This can be very problematic in the more modern, permanently fluid metal TIMs because there is a risk of spilling onto electrical components susceptible to electrical shorting failures. Another common class of TIMs is the elastomeric thermal pads. These TIMs are very spongy and flexible solid pads that push themselves into gaps in the junction due to their resistance to mechanical deformation. The highest TC achieved in this class of TIM in industry, to the knowledge of the authors, is 62.5 W/mK , as reported by the product vendor [37]. Although the TC of these is impressive, they suffer from large contact resistance, which ultimately leads to a modest overall thermal resistance.

Similarly, a solid polymer or clay material can be used in the direct encapsulation of less complex semiconductor circuits than modern VLSI chips for protection from environmental contaminants. Although chips encapsulated in this

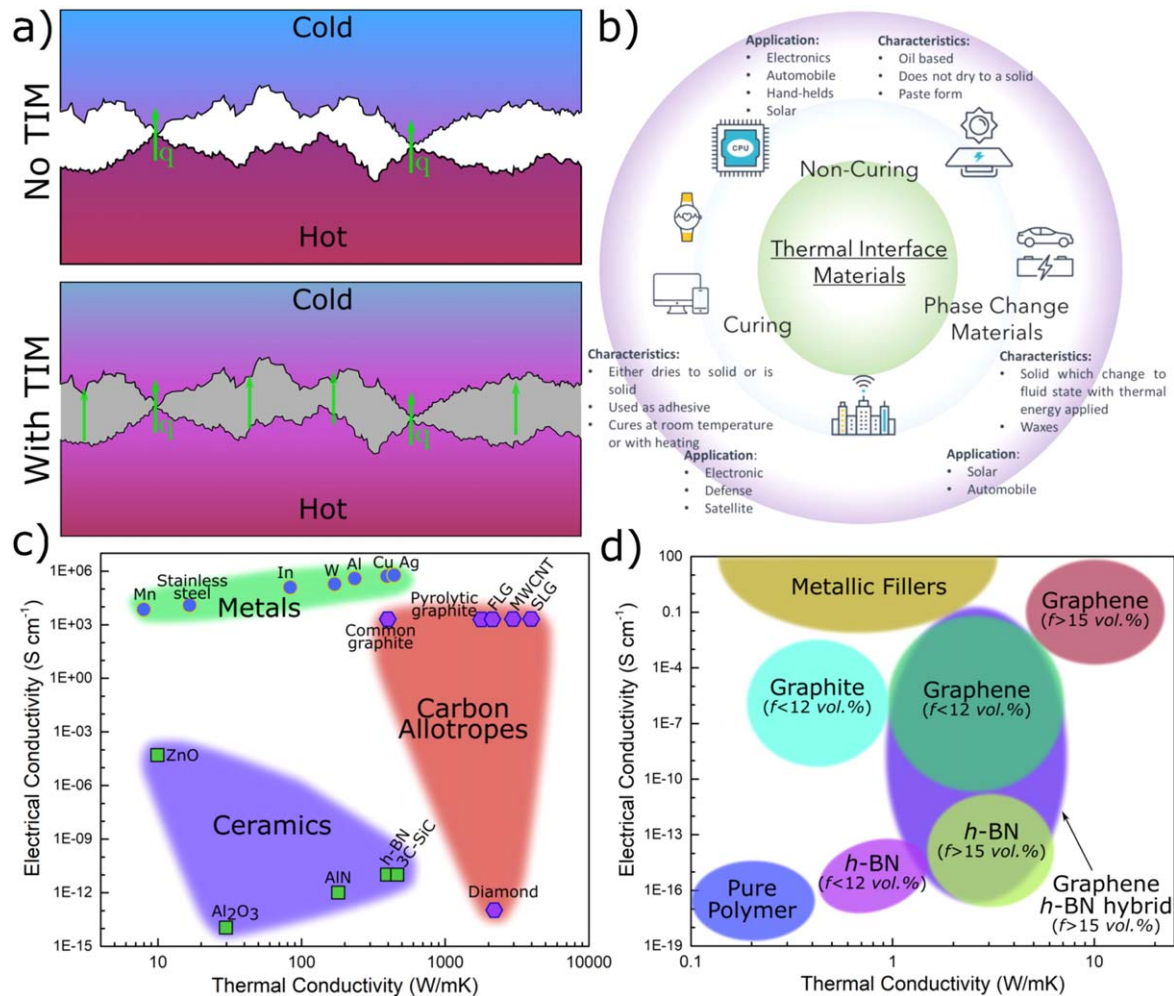


Figure 1. (a) Top: primarily air-gapped exaggerated physical interface in which noteworthy heat dissipation only occurs at a small point of contact. Bottom: same junction after a TIM has been applied allowing substantially more heat dissipation over the otherwise air-gapped regions. (b) Uses for different types of TIMs. (c) Material properties of a selection of popular filler materials. (d) Typical composite properties for different TIMs with un-oriented fillers. [36] John Wiley & Sons. © 2020 WILEY-VCH Verlag GmbH & Co. KGaA, Weinheim.

manner will typically have fewer heat-producing circuit elements than in VLSI chips, devices of this class can include high-power GaN amplifiers with substantial lifespan sensitivity to operating temperature [38]. The thermal performance of the encapsulation material is an important parameter determining device operating temperatures, analogous to a classic TIM. Consequently, chip encapsulation materials are considered a type of TIM. Encapsulation TIMs are typically even more sensitive to electrical conductivity (EC) due to their direct contact with active circuit elements [39]. Figure 1(b) shows different types of TIMs and the applications in which they are typically used.

By far the most common class of TIM is that of the polymeric type. These TIMs have a polymer matrix in which a highly thermally conductive filler is almost always added to form a composite. This class of TIMs has a higher thermal resistance than metal-based TIMs but benefit from being stable at higher temperatures and substantially simpler to work with, especially when re-application is necessary. To date, these TIMs tend to have a lower TC than thermal pads, with a bulk TC in industry between 0.5–7.0 W/mK at high

filler concentration, but have much less contact resistance, leading to overall slightly better performance [40]. It should be noted that the BLT and contact resistance are influenced by the TIM's rheological properties, particularly viscosity, and often increasing the filler loading, thus the TC, of the composite comes at the sacrifice of larger BLT, R_{C1} , and R_{C2} .

Polymeric TIMs have seen considerable research into potential materials that could be used as new conductive fillers. Some common polymers used are mineral and silicone oil, epoxy, poly(methyl methacrylate) (PMMA) and polyethylene [41–43]. The performance of base polymers can vary widely by preparation. For instance, varying the stoichiometric ratio of diglycidyl ether of bisphenol-A (DGEBA)—a common type of epoxy used in this field of research—can result in a factor of two alteration in its thermal diffusivity [44]. One constant requirement of all filler materials is that their physical dimensions must be small enough so that a consistent mixture may be formed within the TIM. Filler materials used either in industry or research include silver, copper, Al_2O_3 , AlN, boron nitride, ZnO, diamond, graphite, carbon nanotubes, few-layer graphene (FLG) and many

others [45–57]. A selection of works into composites filled with these filler materials is summarized in table 1. The legend of acronyms used in table 1 is shown in table 2. Figure 1(c) shows the bulk material properties for a selection of potential filler materials. For each specific geometry of filler, there exists a maximum practical filler loading that can be achieved, often called the workability limit due to an unacceptable increase in composite viscosity [58, 59]. High TIM viscosity can complicate preparation and result in ever-increasing contact resistance in a junction. Typical thermal and electrical properties of composites with randomly oriented fillers of a particular species are shown in figure 1(d).

Research into graphene-filled polymeric TIMs has flourished since the discovery of graphene's extraordinary TC, ranging from 2000–5300 W/mK [152–160]. Early studies showed graphene-filled TIMs with TCs as high as 5 W/mK at room temperature (RT) with graphene filler loading fractions of around 10 vol.%, further spurring graphene TIM research [74, 100]. More recent studies into randomly oriented graphene TIMs in a cured epoxy polymer matrix have achieved TCs of ≈ 12 W/mK [66, 102, 113]. Graphene has promising potential in developing the next generation of TIMs. Counter-intuitively but interestingly, graphene has been included into aerogel and displayed a sharp and unprecedented *reduction* in TC to between 4.7×10^{-3} and 5.9×10^{-3} W/mK at RT, though these results are far from typical for graphene composites [161]. In a closely-related vein of research to that of TIMs, graphene has been composited with thermosetting plastics with the intention of increasing the polymer's fracture resistance, often with little consideration for the composite thermal properties [162].

From a practical standpoint, graphene has the potential to be a cheap filler material due to its composition of abundant carbon, given maturity in synthesis techniques. Liquid-phase exfoliation has stood out as a promising graphene synthesis method with the potential for future economic scaling [163–166]. This technique employs a high-energy sonicator to vibrate the layers of a thick stack of graphite bound by weak van der Waals forces suspended in a fluid apart into few-layer graphene. Another interesting and scalable technique is electrochemical exfoliation in which bulk graphite is used as an electrode and solute ions intercalate into the graphite. This intercalation results in inter-layer stretching that either leads directly to exfoliation or easier exfoliation when it is sonicated [167]. This technique also affords easy functionalization of the resulting graphene flakes. It is also very common and economical to oxidize graphite into graphite oxide via Hummers' method, more simply liquid-phase exfoliates the graphite oxide, then finally reduces the resulting graphene oxide to a form of pure graphene [168–173]. However, these processes have drawbacks primarily resulting in defects that degrade the advantageous properties of the graphene, with substantial defects in the case of graphene derived from the reduction of graphene oxide [174–180].

In TIM research, the term 'graphene' refers to a mix of single-layer graphene and FLG up to a few nanometers in

thickness [181]. Graphene's in-plane TC is reduced with increasing layers up until ≈ 8 total monolayers, at which point the TC stabilizes to that of high-quality graphite at ≈ 2000 W/mK, but still remains more mechanically flexible [182–184]. However, the TC reduction resultant from contact between graphene and a dissimilar material can be far more dramatic [185]. Although there is a reduction of intrinsic TC for increasing graphene layers, there is a competing mechanism to consider where in FLG the outer layers of graphene can insulate interior layers from the substantial TC degradation from phonon scattering that results from contact to other materials, in this case, polymer matrix [186–192]. The 2D geometry of the graphene is an important factor leading to composites composed of graphene having typically much better TC enhancement relative to the 1D carbon nanotube [193]. However, it is important that the graphene exists in the composite with little bending lest it suffer a substantial reduction in performance [194, 195].

Many applications require TIMs with electrically insulating properties. Polymer TIMs can vary widely in their EC depending primarily on the type, concentration and morphology of the filler used. An electrically conductive filler material can be used to fill a polymer TIM for such an application up to a certain level—termed the electrical percolation threshold—where the overall EC of the composite raises orders of magnitude, as can be seen in figure 2(a) [196–200].

Of considerable importance to TIMs, electrical percolation threshold has analogous behavior in TC known suitably as thermal percolation threshold. The percolations of these two material parameters are governed by the concentration and morphology of filler material required for large-scale, uninterrupted paths to become opened up from one filler particle to the next. At this point, a low-resistance pathway, be it thermal or electrical, from one end of the TIM to the other becomes available and each respective property enhances substantially. Figure 2(b) shows two idealized hot and cold surfaces with a filler material between them. In the left schematic, the concentration of spherical fillers is low enough that most fillers are isolated from one another. In the schematic on the right, the concentration is high enough that fillers make contact, forming a long-range pathway from one filler to the next, allowing for a low-resistance pathway between the two surfaces. A common trend in research is to add a second filler material with poor EC to allow the use of a primary, superior thermally conductive but also electrically conductive filler without an unacceptable increase in overall TIM EC [77, 201].

This paper covers recent advances in the promising graphene and graphene/boron nitride hybrid-filled TIMs. It includes a greater in-depth discussion of the thermal percolation threshold and role that adding different types of fillers—often known as hybrid, binary, tertiary, etc filling—can have on it. Also considered is the all-too-often overlooked lifespan performance of these TIMs.

Table 1. TIM thermal conductivity table.

Base polymer	Filler	Cross-plane TC (W/mK)	Measurement method	References
Misc. Fillers				
PDMS	None	0.2	ASTM D5470	[60]
Polyolefin	None	0.3	LFA	[61]
Epoxy	None	0.2-0.22	LFA	[62, 63]
Olefin oil	None	0.145	THW	[64]
Mineral oil	None	0.27-0.3	ASTM D5470	[13, 65]
Epoxy	None	0.17-0.22	LFA	[66–68]
Silver Epoxy	None	1.67	TPS	[69]
Paraffin	None	0.25	TPS	[70]
Aerogel	None	0.18	LFA	[71]
Lauric acid	None	0.215	THW	[72]
Polyamide	None	0.196	LFA	[73]
1-tetradecanol	None	0.32	TPS	[49]
Commercial TIM	Undisclosed	0.52-5.8	ASTM D5470, LFA	[13, 74, 75]
Commercial TIM	added h-BN 2 wt.%/6 wt.%	0.56/.64	ASTM D5470	[75]
Epoxy	AlN 60/74 vol.%	3.8/8.2	ASTM D5470 similar	[76]
Epoxy	h-BN 43.6 vol.%	3.46	LFA	[77]
Epoxy	h-BN 2.9 vol.%/45 vol.%	0.32/5.5	TPS, LFA	[66]
Epoxy	h-BN 15 vol.% (CPA)	6.1	TPS	[78]
Epoxy	h-BN 44 vol.%	9.0	LFA	[79]
Epoxy	h-BN 34 vol.%	4.4	LFA	[80]
Epoxy	h-BN 30 wt.%	0.6	LFA	[81]
Epoxy	h-BN 40 vol.% (CPA)	5.5	LFA	[82]
Epoxy	h-BN 20 vol.%	1.2	LFA	[83]
Epoxy	h-BN 50 vol.% (functionalized)	9.81	LFA	[84]
Epoxy	AlN 50 vol.%	1.21	TPS	[85]
Epoxy	Silica 50 vol.%	0.58	ASTM E1530	[45]
Epoxy	SiC 72 wt.% (functionalized)	5.75	LFA	[86]
Polyimide	h-BN 7 wt.%	3	LFA	[87]
Polyimide	h-BN 60 wt.%	7.0	TPS	[88]
Polyimide	h-BN 60 wt.%	5.4	TWA	[89]
Polyimide	h-BN 30 wt.%	0.72	LFA	[90]
PBT	h-BN 70 vol.% (functionalized)	11	LFA	[91]
PMMA	h-BN 80 wt.% (functionalized)	10.2	LFA	[91]
PCL	h-BN 20 wt.%	1.96	LFA	[92]
PVA	h-BN 30 wt.%	4.41	LFA	[93]
PVA	h-BN 10 wt.% (functionalized)	5.4	LFA	[94]
1-tetradecanol	Ag nanowires 11.8 vol.%	1.46	TPS	[49]
Silicone Oil	ZnO nanoparticles 18.7 vol.%	0.44	TPS	[53]
Silicone Oil	Zno columns 18.7 vol.%	0.55	TPS	[53]
Silicone Oil	ZnO Czech hedgehog structure 18.7 vol.%	0.83	TPS	[53]
Resin	SiC 25 wt.%	1.28	Unique method	[95]
Non-graphene carbon fillers				
Epoxy	Small graphite 4 wt.%/13 wt.%/20 wt.%	0.22/0.65/4.3	LFA	[63]
Epoxy	Large graphite 4 wt.%/13 wt.%/20 wt.%	0.87/2.95/4.3	LFA	[63]
Epoxy	CF 20 wt.% (non-heated/heated)	0.35/3.75	LFA	[63]
Epoxy	Graphite 10 wt.%	0.5	LFA	[96]
Epoxy	MWCNT 20 wt.%	0.4	LFA	[97]
Epoxy	Graphite nanoplatelet (non/functionalized) 10 wt.%	0.65/1.75	LFA	[86]
Epoxy	Graphite 5.4 vol.% (thicknesses 60 nm/30 nm/4 nm)	1.1/1.35/1.43	ASTM C518	[62]
Epoxy	Graphite nanoplatelet 14 wt.%	0.73	ASTM D5470	[98]
Silicone oil	Graphite nanoplatelet 14 wt.%	0.5	ASTM D5470	[98]
Hatcol 2372	Graphite nanoplatelet 14 wt.%	0.48	ASTM D5470	[98]
Epoxy	SWCNT 1 wt.%	0.49	ASTM D5470 similar	[99]
Epoxy	Graphite 44.3 wt.%	1.7	TPS	[100]
Oil	MWCNT 1 vol.%	0.36	THW	[64]

Table 1. (Continued.)

Base polymer	Filler	Cross-plane TC (W/mK)	Measurement method	References
CPE	SWCNT 50 wt.%	1.6	TDTR	[101]
Silver epoxy	CB 5 vol.%	2	TPS	[69]
	Graphene fillers			
Epoxy	GnP 20 wt.%	1.5	LFA	[97]
Epoxy	Graphene 10 vol.%	5.1	LFA	[74]
Epoxy	Graphene 11.4 vol.%/43.6 vol.%	1.9/8.0	LFA	[77]
Epoxy	Graphene 2.7 vol.%/44.6 vol.%	0.49/11.4	LFA	[66]
Epoxy	Graphene 55 wt.% (thicknesses 3 nm/ 12 nm)	3.3/8	LFA	[102]
Epoxy	Graphene 1 wt.% (RA/CPA)	0.2/0.35	LFA	[103]
Epoxy	GnP 2 wt.% (functionalized)	0.52	LFA	[104]
Epoxy	Graphene 10 wt.% (functionalized)	1.53	LFA	[96]
Epoxy	rGO 2 wt.%	0.24	LFA	[68]
Epoxy	Graphene 1 wt.% (RA/CPA/IPA)	0.4/0.57/0.25	LFA	[67]
Epoxy	Graphene 0.92 vol.% (CPA)	2.13	LFA	[105]
Epoxy	Graphene 10 wt.%	0.67	LFA	[106]
Epoxy	Graphene 30 wt.%	4.9	LFA	[107]
Epoxy	Graphene 10 vol.%	3.35	LFA	[108]
Epoxy	GnP 8 wt.%	1.18	LFA	[109]
Epoxy	GnP 10 wt.%	6.5	LFA	[110]
Epoxy	Graphene alone/with PMMA 1 wt.%	0.6/1.4	ASTM D5470 similar	[111]
Epoxy	Graphene 5/10 vol.%	2.8/3.9	ASTM D5470 similar	[112]
Epoxy	GnP 25 vol.%	6.75	ASTM C518	[62]
Epoxy	Graphene 24 vol.%	12.4	DSC	[113]
Epoxy	Graphene 10.1 wt.%	4.0	TPS	[100]
Polyamide	rGO wt.%	0.416	LFA	[73]
Polyamide	rGO 5 wt.% (functionalized)	0.41	LFA	[114]
Polyamide	rGO 8 wt.% (non/functionalized)	3.34/5.1	TPS	[9]
Polyurethane	rGO 1.04 wt.%	0.8	LFA	[115]
Polyimide	Graphene 12 wt.%	0.41	LFA	[116]
Cellulose	rGO 30 wt.% (IPA)	0.07	LFA	[117]
Mineral oil	Graphene 10 wt.%/20 wt.%/40 wt.%	3.1/4.8/6.7	ASTM D5470	[13]
Mineral oil	Graphene 27% vol.%	7.1	ASTM D5470	[65]
Silver epoxy	Graphene 1 vol.%/5 vol.%	4.0/9.9	TPS	[69]
Paraffin	Graphene 0.5 wt.%/1 wt.%/20 wt.%	10/15/45	TPS	[70]
Commercial TIM	Added graphene 2 wt.%/4 wt.%/6 wt.%	0.7/0.75/0.8	ASTM D5470	[75]
Commercial TIM	Added graphene 2 vol.%	14	LFA	[74]
Polystyrene	Graphene 20 wt.%	0.48	LFA	[118]
Aerogel	rGO 20 vol.%	2.64	LFA	[71]
PDMS	Graphene 0.5 wt.% (scaffolded)	0.4	ASTM D5470	[60]
Polyolefin	Graphene 10 wt.%	5.6	LFA	[61]
Eicosane	Graphene 10 wt.%	2.0	TPS	[119]
Lauric acid	GnP 1 vol.%	0.49	THW	[72]
Methyl vinyl silicone	rGO 1.5 wt.%	2.7	LFA	[10]
PVDF	rGO 0.25 wt.%	2.35	LFA	[120]
	Hybrid fillers			
Epoxy	Graphene 21.8 vol.%, h-BN 21.8 vol.%	6.5	LFA	[77]
Epoxy	GnP 40 wt.%, Cu-NP 35 wt.%	13.5	LFA	[121]
Epoxy	MWCNT grown on GnP 20 wt.%	2.4	LFA	[97]
Epoxy	AlN nanowires 30 vol.%, AlN spheres 30 vol.%	5.23	LFA	[122]
Epoxy	BN nanowires 12.8 vol.%, BN spheres 30 vol.%	3.6	LFA	[123]
Epoxy	Al ₂ O ₃ -attached GnP 12 wt.%	1.49	LFA	[124]
Epoxy	Ag-attached h-BN 25.1 vol.%	3.1	LFA	[125]
Epoxy	Graphene oxide 49.6 wt.%, MWCNT 0.4 wt.%	4.4	LFA	[126]
Epoxy	h-BN, SiC 40 vol.% total (CPA)	5.77	LFA	[127]
Epoxy	h-BN, rGO 13.2 wt.% total (CPA)	5.1	LFA	[128]
Epoxy	MWCNT 5 wt.%, SiC 55 wt.%	6.8	LFA	[129]
Epoxy	AlN 40.9 wt.%, Al ₂ O ₃ 17.5 wt.%	3.4	LFA	[130]
Epoxy	rGO 20 wt.%, graphene 10 wt.% (scaffolded)	6.7	LFA	[131]

Table 1. (Continued.)

Base polymer	Filler	Cross-plane TC (W/mK)	Measurement method	References
Epoxy	AlN 25 vol.%, MWCNT 1 vol.%	1.21	TPS	[85]
Epoxy	Graphene oxide 6 wt.%, AlN 50 wt.%	2.77	TPS	[132]
Epoxy	MWCNT 4 wt.%, AlN 25 wt.%	1	TPS	[133]
Epoxy	MWCNT 15 wt.%, Cu 40 wt.%	0.6	TPS	[134]
Epoxy	Graphene 0.9 wt.%, MWCNT 0.1 wt.%	0.3	TPS	[135]
Epoxy	Silica-coated AlN 50 vol.%	1.96	ASTM E1530	[45]
Epoxy	Graphene 16 vol.%, h-BN 1 vol.%	4.72	DSC	[113]
Epoxy	Ag nanowires 4 vol.%, Al ₂ O ₃ 15 wt.%	1.08	TPS similar	[136]
Epoxy	Graphene 1.5 wt.%, MgO 30 wt.%	0.51	ASTM D5470 similar	[137]
Epoxy	MgO-coated graphene 7 wt.%	0.4	ASTM C518	[138]
Epoxy	Al ₂ O ₃ 30 wt.%, rGO 0.3 wt.%	0.33	ASTM E1461	[139]
Epoxy	Graphene oxide-encapsulated h-BN 40 wt.%	2.2	ASTM D5470	[140]
Polyimide	h-BN (μm scale) 21 wt.%, h-BN (nm scale) 9 wt.%	1.2	TPS	[141]
Polyimide	BN-coated Cu nanoparticles, nanowires 10 wt.% total	4.3	TPS	[142]
Polyimide	BN 50 wt.%, graphene 1 wt.%	2.11	ASTM D5470	[143]
Polyamide	Graphene 20 wt.%, h-BN 1.5 wt.%	1.76	LFA	[118]
Polyamide	Graphene oxide 6.8 wt.%, h-BN 1.6 wt.%	0.9	LFA	[144]
Polycarbonate	GnP 18 wt.%, MWCNT 2 wt.%	1.39	TPS	[145]
PDMS	Graphene (scaffolded), CB 2 wt.%/8 wt.%	0.41//0.7	ASTM D5470	[60]
PPS	h-BN (μm scale) 40 wt.%, h-BN (nm scale) 20 wt.%	2.64	TPS	[146]
PPS	h-BN 50 wt.%, MWCNT 1 wt.%	1.74	TPS similar	[147]
PVA	Graphene, MWCNT each Ag-attached 20 vol.% total	12.3	LFA	[148]
Polystyrene	GnP 20 wt.%, h-BN 1.5 wt.%	0.66	LFA	[118]
PVDF	GnP 5 wt.%, nickel 8 wt.%	0.66	LFA	[149]
Cyanate ester	Graphene 5 wt.%, iron-nickel alloy 15 wt.%	4.1	TPS	[150]
Poly(lactic acid)	Alumina 70 wt.%, graphene 1 wt.%	2.4	TPS	[151]

2. Recent advances in graphene TIMs

Some of the most thermally conductive polymeric TIMs have employed the quasi-2D graphene as filler material, occasionally including a second filler as an additional component. Normally, filler materials are in general randomly oriented by a classic mixing procedure. This random orientation of fillers is less efficient at increasing composite TC than if directionally-selective processes are employed. Preferential orientation of high aspect ratio fillers serves to effectively increase the size of the flake along the dimension of interest and allows for greater unobstructed heat pathways. Studies concerned with selectively aligning graphene fillers have proved to be useful in increasing TC improvement per graphene loading level [202].

To the knowledge of the authors, the first work on TIMs with graphene-like materials used as a filler was conducted by Fukushima *et al* in 2006 [62, 169, 203]. This work started with typical, macroscopic graphite that was oxidized and then exfoliated. The thickness of the obtained filler material was ≈ 10 nm with lateral dimensions of $\approx 15 \mu\text{m}$, a geometric portfolio typically referred to as ‘few-layer graphene oxide’ today.

Tremendous interest in graphene as a filler of TIMs followed an early demonstration of a TC enhancement of 2300% at only 10 vol.% filler loading in an epoxy matrix [74], as shown in figure 3(a). These levels of TC enhancement have since been confirmed by independent studies [100, 113]. Figure 3(b) shows that the composites exhibit a reduction in TC as their temperatures are increased. This behavior is consistent with Umklapp process-limited crystalline materials. The increased dependence of TC on temperature with higher loading samples shows the increasing reliance of the composite’s heat flow on graphene. Also studied was an unprecedented enhancement of a commercial TIM from ≈ 5.8 to 14 W/mK with a small addition of 2 vol.% of graphene. The Maxwell Garnett effective medium approximation, which is known to be effective for lower loading fractions was used to analyze the data [204, 205]. By treating graphene and carbon nanotubes as dramatically oblate and prolate spheroids, respectively, superior TC of graphene composites is effectively modeled [74]. The following is the derived expression for a graphene-filled composite’s TC:

$$K = K_p \left[\frac{3K_m + 2f(K_p - K_m)}{(3 - f)K_p + K_m f + \frac{R_B K_m K_p f}{H}} \right], \quad (2)$$

Table 2. Table acronym legend.

Acronym	Meaning
PDMS	Poly(dimethylsiloxane)
LFA	Laser flash analysis
TPS	Transient plane source
RA	Randomly aligned filler (studies without any alignment classification are randomly oriented)
CPA	Cross-plane filler preferential alignment
IPA	In-plane filler preferential alignment
TWA	Temperature wave analysis
PBT	Polybutylene terephthalate
PCL	Poly(caprolactone)
PVA	Poly(vinyl alcohol)
PMMA	poly(methyl methacrylate)
CF	Carbon fiber
MWCNT	Multi-walled carbon nanotube
SWCNT	Single-walled carbon nanotube
THW	Transient hot wire
CPE	Conjugated polyelectrolytes
TDTR	Time-domain thermoreflectance
CB	Carbon black
GnP	Graphene nanoplatelet
rGO	Reduced graphene oxide
PVDF	Poly(vinylidene fluoride)
PPS	Poly(phenylene sulfide)

where R_B is the microscopic interfacial resistance between graphene and the matrix, K_p is the TC of the flakes, K_m is the TC of the matrix, f is the loading fraction and H is the thickness of the flakes.

In all TIMs, one must consider the microscopic interfacial (Kapitza) resistance of fillers within the material, a factor quite analogous to the macroscopic contact resistance that the TIM is employed to ameliorate. There is an unfortunate mismatch of phonon vibrational frequencies between graphene and polymer matrix that functionalization can address [206–209]. Using this technique, Song *et al* achieved a TC of 1.53 W/mK in an epoxy resin polymer with 10 wt.% of functionalized graphene [96]. It has been shown in molecular dynamics simulations, effective medium theory, and others that the reduction of microscopic filler interfacial resistance resulted in an increase of overall composite TC [210–215]. Figures 4(a) and (b) show schematics of a linear hydrocarbon chain grafted to a graphene sheet to produce a functionalized surface. In figure 4(c), the TC, K^* , of a simulated composite is analyzed at varied graphene lateral dimensions with different hydrocarbon areal densities, σ , on the graphene flakes. Interestingly, the functionalized graphene composites achieved higher TC until a filler length of $\approx 5 \mu\text{m}$, at which point the preservation of non-functionalized graphene TC proved to be more impactful than thermal coupling between graphene and polymer matrix. Shen *et al* also directly examined the benefit of functionalization versus graphene size with similar findings [216]. It was determined that functionalization can inhibit composite TC by negatively affecting large graphene flake intrinsic TC, establishing a critical flake size at which point any larger flakes would result in composites being negatively impacted by the process.

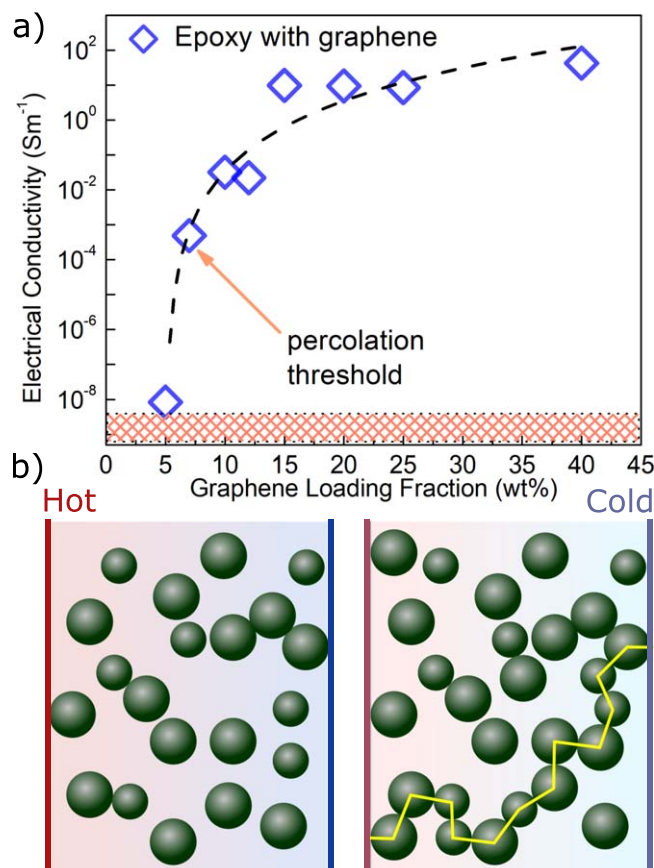


Figure 2. (a) EC of a composite above and below the electrical percolation threshold with electrically conductive graphene fillers. (b) Left: TIM between a hot and cold surface with low filler loading with natural size variations. Right: same scenario with more fillers and the development of a low-resistance percolation pathway. [114] John Wiley & Sons. © 2019 WILEY-VCH Verlag GmbH & Co. KGaA, Weinheim.

Alternatively, graphene functionalization can be useful to prevent agglomerations and to attach components that can be used to orient the graphene flake [103].

Using typically very defected graphene derived from the reduction of graphene oxide, Ding *et al* observed an improvement of 0.196 to 0.416 W/mK in polyamide with a graphene loading of 10 wt.% [73]. In this study, a surface functionalization process was conducted, aiming to increase the thermal coupling between the reduced graphene oxide and the polymer matrix. Using a similar reduced graphene oxide at only 1.5 wt.% and an additional functionalization step, Zhang *et al* achieved a TC of 2.7 W/mK in a silicone matrix [10]. This TIM was then applied to bridge an LED chip and a heat sink with a smaller temperature difference between the two as the TIM TC increases. Cho *et al* used graphene derived from graphene oxide and a polyamide matrix to create a composite with a TC of 3.34 W/mK at 5 wt.% [9]. Functionalization has been applied to graphene composites using gallic acid to attach a monomer and help with the dispersion of graphene in DGEBA [217]. In a similar research strategy, functionalization was used to attach silver particles to graphene to also prevent graphene agglomeration [136].

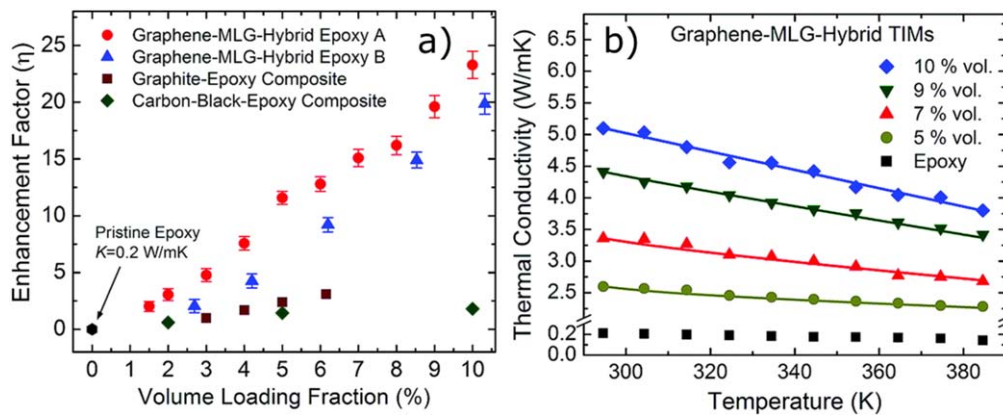


Figure 3. (a) Enhancement of pure epoxy with increasing load level up to 10 vol.%. ‘Graphene-MLG-Hybrid Epoxy A’ corresponds to a composite that was mixed for ≈ 12 h at 15 000 RPMs and ‘Graphene-MLG-Hybrid Epoxy B’ corresponds to a less mixed composite that went through ≈ 10 h of 5000 RPMs of mixing. (b) Temperature-dependent TC for graphene and few-layer graphene TIMs at different load levels. Reprinted with permission from [69]. Copyright (2012) American Chemical Society.

Researchers have used graphene functionalization to attach magnetic particles, such as Fe_3O_4 , to the sheets. Then, once the functionalized graphene is dispersed within the polymer a magnetic field is applied. Because the graphene sheets are attached to the magnetic particles, they are aligned along the magnetic field, leading to the ability to increase the thermal transport along a particular direction. With an epoxy polymer matrix, Yan *et al* raised the TC of a polymer from 0.17 to 0.41 W/mK with the addition of 1 vol.% randomly oriented graphene [67]. However, when the graphene was functionalized with Fe_3O_4 and magnetically aligned, the composite achieved an approximate TC of 0.57 W/mK when aligned parallel to the direction of thermal characterization and 0.25 W/mK when perpendicular. A similar study was conducted by Renteria *et al*, with the graphene source material shown in figure 5(a). Figure 5(b) shows the clear magnetic behavior exhibited by the graphene functionalized by Fe_3O_4 . The material was magnetized between two copper foils and on top of a permanent magnet, as shown in figure 5(c). TEM microscopy revealed the attachment of the particles in 5(d). An optical microscopy image showing the load level of the composite being low enough to pass light is shown in figure 5(e). The TCs are shown in figure 5(f), verifying previous results that orienting graphene in this manner is more efficient at enhancing the TC than when using a random orientation approach [103]. Alternatively, the alignment of graphene has been achieved by Huang *et al* through the clever use of interfaces between two different polymer materials to preferentially trap graphene sheets at the interface [218]. This serves to both locally increase the loading level and allow for directional orientation along the interface. Another intentional filler orientation work by Lian *et al* reported a TC of 2.13 W/mK, an enhancement of 1231%, with only 0.92 vol.% of graphene [105]. Recently, graphene alignment by way of a freeze-casting method that uses ice crystals to preferentially orient the flakes has grown in popularity [219–223]. An interesting technique to realize semi-controllable graphene orientation is to fix graphene to a

3D structure, with a morphology similar to sponges, then cure the graphene with or without the scaffold in a polymer of choice [224, 225].

The directional control of graphene fillers is primarily of interest because of its potential to achieve order-of-magnitude improvement over current composites in the cross-plane direction (from source to sink). Selective alignment along the plane of a TIM—that is, perpendicular to the surface normal of the heat-producing device—remains an area of important inquiry. However, this has fewer immediately practical implications as these composites are not well-suited for the transfer of heat to a heat sink [226]. General TIM composite techniques tend to naturally result in greater in-plane TC than in the cross-plane direction, as can be seen in most studies that measure in both directions [114, 227]. In very thin composites of tens to hundreds of μm in thickness, often referred to as ‘paper TIMs’, the in-plane TC can be greater than in the cross-plane direction by orders of magnitude due to the in-plane orientation of fillers [116, 117, 226, 228–234].

Prolongo *et al* analyzed the thermal performance increase that resulted from filling DGEBA with graphene [106]. In this work, a modest enhancement of TC was observed relative to what others would find with a similar loading fraction of 10 wt.% graphene fillers of 0.67 W/mK, compared to 0.18 W/mK measured of the pure epoxy. Similar results were obtained previously with a TC of 0.65 W/mK with a similar filler, loading level and polymer matrix [86]. In each of these instances, the graphene lateral dimensions were relatively small, as small as 3 μm , often requiring thermal dissipation to traverse through the highly-insulating matrix. In addition, graphene intrinsic TC diminishes with reducing the lateral size even if larger than the gray phonon mean free path of ≈ 750 nm [153, 235]. Since functionalization can aid in the thermal coupling between graphene and matrix, if small flakes are used the benefit of functionalization is more pronounced.

Park *et al* fabricated epoxy polymer TIMs cured directly into an ASTM D5470-inspired copper interface for testing [112]. An interfacial resistance of 3.2 and 4.3 $\text{mm}^2\text{K/W}$ for 5

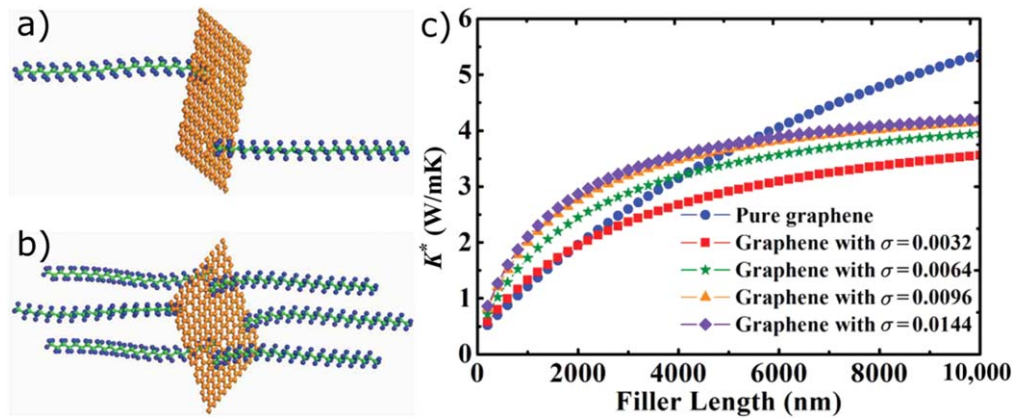


Figure 4. (a) Section of a graphene flake with two linear hydrocarbon chains grafted on. (b) Six linear hydrocarbons grafted onto graphene. (c) Non-equilibrium molecular dynamics simulation composite TC with different areal densities of grafted hydrocarbons (σ) per square angstrom. Increasing the density of hydrocarbon attachments results in better performance until the length of graphene approaches approximately 5 microns, at which point the intrinsic graphene TC reduction becomes a more dominant mechanism in the composite. Reproduced from [126]. CC BY 3.0.

and 10 vol.%, respectively, was measured at 330 K. The TC of each sample was measured to be 2.8 and 3.9 W/mK. These findings highlight the need to consider the potential increases in R_{C1} and R_{C2} resultant from a corresponding increase in viscosity due to an increased filler level. This outcome of the superior thermally conductive composite having a greater interfacial resistance was observed elsewhere in a polyolefin polymer matrix and was attributed to its mechanical properties [61].

Using graphene derived from chemical vapor deposition and subsequent exfoliation, a method that produces graphene of typically greater quality than that from the reduction of graphene oxide, a TC of 4.9 W/mK was achieved with a 30 wt.% loading in an epoxy resin [107]. In addition, the TC was examined at different temperatures. There is a reduction of performance at higher temperature, as one would expect and has been observed elsewhere, but the extent of the reduction proved to be modest, showing promising signs for thermal stability. Wang *et al* similarly studied an epoxy composite with 8 wt.% of graphene and achieved a 627% improvement in TC, resulting in 1.18 W/mK [109]. The performance of composites based on these constituent materials can vary substantially from researcher to researcher, displaying the great many influencing parameters that determine their properties. At a similar graphene loading of 8 wt.%, Moriche *et al* reported a TC of ≈ 0.5 W/mK in an epoxy composite [110]. These influencing factors that can alter composite performance, range from being intentional and knowable to being difficult to identify.

Generally, graphene without defects is desirable because its TC reduces with increased defect density. However, Liu *et al* showed in a non-equilibrium molecular dynamics simulation a mechanism for *increased* TC in a liquid n-octane and graphene composite with increasing vacancy defects [236]. Upon introducing vacancy defects to graphene at concentrations up to 8%, the thermal conductance of the composites is increased because the graphene fillers become more structurally flexible, with a corresponding decrease in its

in-plane and out-of-plane phonon frequency. This reduction in out-of-plane vibrational frequency aids in the thermal coupling of the graphene and polymer. This highlights the need to take holistic considerations when designing a composite as opposed to what is traditionally good for an individual component of the composite. Viewing this and other works suggest that defect-based enhancements depend on the type of defect and polymer type [237].

An interesting and relatively recent strategy has been to attach graphene to another larger material to achieve a desired larger-scale placement and orientation. This technique was used by Eksik *et al* to make PMMA balls coated with graphene that were then used to fill an epoxy [111]. SEM micrographs of varying graphene loadings and magnifications are shown in figures 6(a) and (b). Using this technique, the researchers achieved ≈ 1.4 W/mK at 1 wt.%, versus only ≈ 0.6 W/mK of equivalent loading graphene without PMMA grafting, as shown in figure 6(c). A similar idea was applied by Li *et al* to attach reduced graphene oxide to thermoplastic polyurethane balls and then hot-press mold the balls together, achieving a TC of 0.8 W/mK at 1.04 wt.% [115].

Graphene fillers have been applied to phase-change materials, often used in TIMs and thermal energy storage [238]. An aerogel material's TC has been increased from 0.18 to 2.64 W/mK with the inclusion of approximately 20 vol.% of graphene oxide [71]. The phase-changing polymer icosane's TC was enhanced by a factor of 400% to ≈ 2.1 W/mK through the inclusion of 10 wt.% of graphene by Fang *et al* [119]. These results will allow for better temperature uniformity within each phase-changing polymer due to the enhanced heat flow characteristics with strong implications in the ever-more-important lithium battery field [70]. In figure 6(d), an SEM micrograph of a prepared graphene and paraffin composite is shown. In figure 6(e), TCs of different graphene-enhanced composites for realistic battery temperatures are presented with >45 W/mK performance at slightly above RT. Graphene types A, B, and C in this figure correspond to increasing thicknesses of graphene, from mostly

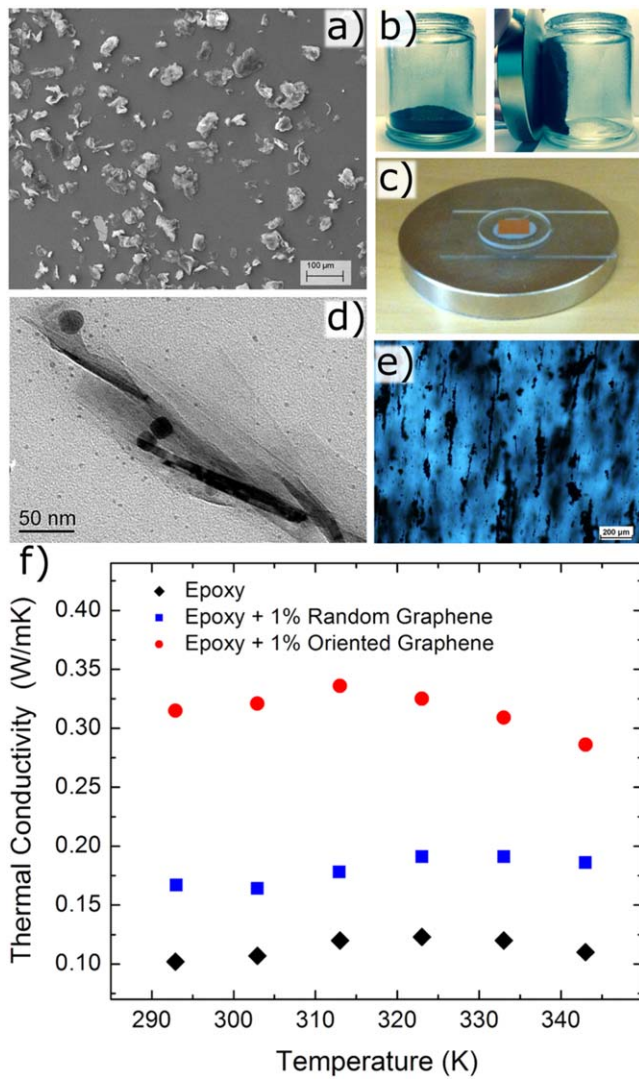


Figure 5. (a) SEM image of graphene derived by liquid-phase exfoliation. (b) Photograph showing the response to the magnetically-functionalized graphene powder to an applied magnetic field. (c) Functionalized graphene between two copper foils and placed on a permanent magnet for filler alignment. (d) TEM micrograph of graphene flake with attached Fe_3O_4 . (e) Optical microscopy image with low concentration of aligned filler. (f) Apparent TC at different temperatures. The superiority of intentionally oriented graphene flakes to randomly orientated graphene and pure epoxy is evident. Reprinted from [133], Copyright (2015), with permission from Elsevier.

single-layer to an average thickness of 8 nm. In a lauric acid phase-change material, a TC enhancement of 230% was obtained with as little as 1 vol.% [72].

3. Percolation

When a composite is loaded past a critical level, there is a precipitous increase in conductive ability, whether it be electrical or thermal, as mentioned previously and illustrated in figure 2. This occurs because as the concentration of conductive filler particles increases eventually full pathways from filler to filler form to allow large-scale, low-resistance

networks through the composite. Electrical percolation of composites employing electrically conductive fillers such as metals or carbon allotropes is very strongly supported by research [99, 169, 239–242]. The EC of composites is well described by a power law, $\sigma \approx (f - f_E)^t$, where σ is the EC, f is the filler volume fraction, f_E is the percolation threshold loading level and t is the critical exponent.

The exact nature and efficacy of thermal percolation in composites were until recently not considered a settled issue in science [64, 159, 243–249]. It is clear that the change of composite thermal properties that results from percolation is more modest than that of EC, which can span over ten orders of magnitude, strongly depending on the matrix and fillers used [77]. The less obvious observable signs of thermal percolation relative to electrical percolation are often attributed to the simple fact that the span of available materials' TC is far more constrained than in the case of EC. The dynamic range of TC—a total ratio of $K_f/K_m \approx 10^5$ —in materials that one could use in practical applications is much lower than that of EC—a total ratio of $\sigma_f/\sigma_m \approx 10^{15}$, resulting in effectively no pre-percolated polymer electrical conduction while still providing some thermal conduction [66, 244]. Since the ratio of K_f/K_m is often ten orders of magnitude less than σ_f/σ_m , the TC enhancement at the percolation threshold is less precipitous than EC enhancement at its respective percolation threshold.

More recent works have more conclusively shown the onset of thermal percolation in graphene and *h*-BN composites [66, 249]. Figures 7(a) and (b) show TC performance of graphene and *h*-BN showing superlinear TC enhancement after a certain filler loading fraction—the percolation threshold [243, 246–252]. The thermal percolations were observed at about 30 vol.% in the graphene composites and 23 vol.% in the *h*-BN composites. The enhancement of TC as the loading fraction is increased, was fitted to Maxwell Garnett, Agari, and finally with a fantastic agreement, the semi-empirical Lewis–Nielsen model [253–257]. This specific behavior is somewhat different from a previous study by Shtein *et al* into graphene composite percolation in which pre-percolation behavior was found to match Nans' model and post-percolation matched the adjusted critical power law [249, 258]. The Lewis–Nielsen TC model is,

$$\frac{K}{K_m} = \frac{1 + ABf}{1 - B\Psi f}, \quad (3)$$

where A is equal to $k_E - 1$ where k_E is the generalized Einstein coefficient, $B = (K_f/K_m - 1)/(K_f/K_m + A)$, and $\Psi = 1 + ((1 - \phi_m)/\phi_m^2)f$ where ϕ_m is the maximum packing fraction [259]. The values of parameters A and ϕ_m are unknown for quasi-2D fillers such as graphene and *h*-BN, and were treated as fitting parameters.

It was found that loading beyond the thermal percolation threshold placed considerable importance on the cross-plane TC of the graphene fillers because thermal transport in this direction facilitated the passing on of heat from one flake to the next in the percolation network. The graphene composites exhibited consistently higher TC than their *h*-BN counterparts. This is due to the superiority of graphene intrinsic TC

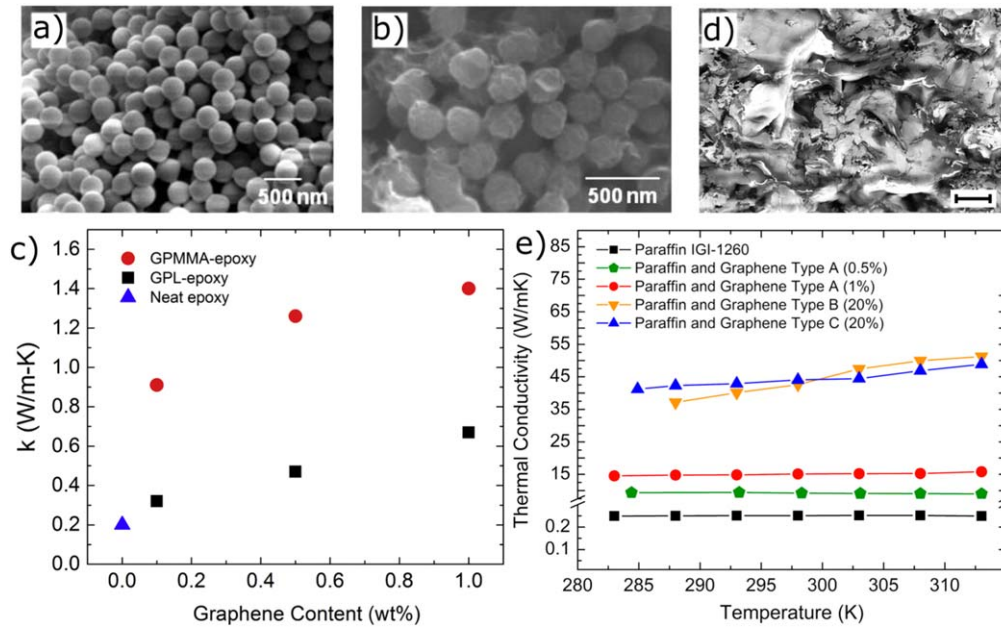


Figure 6. In this study, graphene was grafted onto PMMA spheres to provide structure to the graphene. (a) SEM image of pure PMMA spheres. (b) PMMA spheres with 16 wt.% graphene. (c) TC results of graphene attached to PMMA spheres (GPMMA) as red dots and graphene without PMMA attachment (GPL) as black squares. (d) SEM micrograph of graphene and phase-change material. (e) TC performance of graphene-enhanced paraffin over realistic battery temperatures. (a)–(c) Reprinted from [170], Copyright (2016), with permission from Elsevier. (d) and (e) Reprinted from [171], Copyright (2014), with permission from Elsevier.

relative to that of *h*-BN, at a still impressive experimentally-determined TC of ≈ 230 to ≈ 480 W/mK at RT and up to ≈ 1000 W/mK when determined theoretically [260–266].

Using the Lewis–Nielsen model, a surprisingly low *apparent* TC of ≈ 37 W/mK was determined for the graphene materials used inside the TIM. This lower-than-expected TC was attributed to the unexpectedly important impact of filler cross-plane TC to the overall thermal transport. If the composite is filled past its percolation threshold, much of its heat will be transporting from one flake to another lying on top of it, forcing transport in the cross-plane direction. TC in this direction can be two orders of magnitude less than in the in-plane direction. It is also possible that the matrix and filler defects can induce phonon scattering that negatively affects the TC. However, the amount of scattering necessary to alone explain the low *apparent* TC of graphene is less likely. The effect of microscopic contact resistance—Kapitza resistance—is likely a contributor and could be greatly diminished in future works with functionalization processes [267–269].

Figure 7(c) shows a comparison of thermal transport for different composite parameters from a finite element heat diffusion numerical simulation. The subset schematic in figure 7(c) shows a quasi-2D filler within an epoxy matrix. This filler has heat applied and that heat is transported via diffusion away from the schematic's exposed face towards the end of the flake. Then, the heat traverses primarily vertically through the epoxy, across a distance d , and into another filler. Plotted in (7c) is the thermal flux of flakes with high-quality graphite in-plane TC of 2,000 W/mK and various cross-plane TCs with different distances between the adjacent flakes. Evident from the plot is the considerable importance of the overall thermal flux, amounting to a factor of ≈ 5 , on the

cross-plane TC when the fillers are making contact, such as in the thermal percolative state. In figure 7(d) the total thermal flux versus distance between flakes is considered for varying flake lateral sizes and fixed thicknesses. The importance of large flakes below the percolation threshold, and thus large inter-planar distance, is clear and is due to the opening of long, low-resistance pathways and the reduction of reliance on the comparatively low cross-plane TC.

Recently, a new composite TC differential equation model was reported that agrees well with this work [270]. The model is written as,

$$\frac{dX}{d\phi} = \frac{1}{1-\phi} \left[\frac{R_1(1-\Lambda)}{3} + \frac{B\Lambda(R_2-X)X}{R_2+(B-1)X} \right], \quad (4)$$

where X is the ratio of the final composite thermal TC to the pure matrix TC, ϕ is the filler volume fraction, R_1 and R_2 are the ratios of the filler effective TCs to that of the matrix, Λ is the volume fraction of particles that are in tight clusters as a result of imperfect mixtures, and B characterizes how particles and their clusters deviate from a spherical shape. With this model, we are aware of thermal boundary resistances, percolative networks, and imperfect mixture agglomerations.

4. High-loading non-curing graphene thermal interface materials

Cured, solid-form TIMs receive more attention in research possibly because of the ease of working with them relative to non-curing forms, in addition to their direct comparison to chip encapsulation materials. However, a more representative comparison between the TIMs used in the VLSI package and

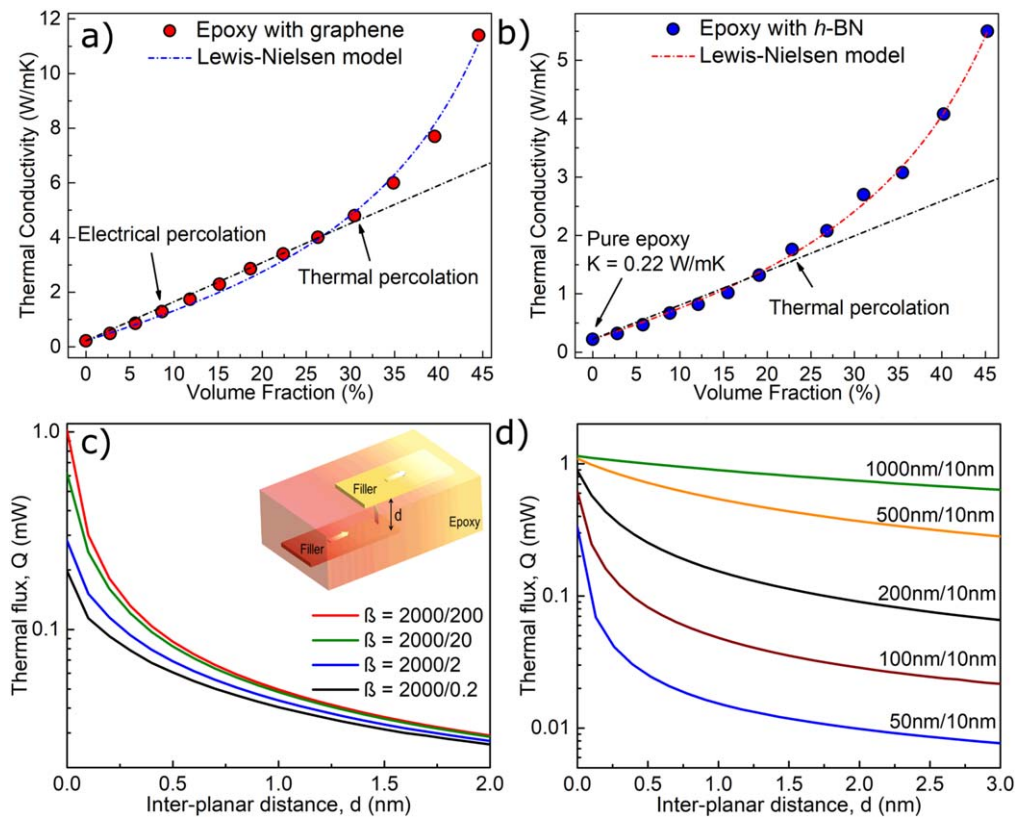


Figure 7. TC versus volume fraction with linear and Lewis–Nielsen trend lines for comparison. (a) Graphene composites. (b) h-BN composites. Superior TC of graphene composites compared to h-BN composites is attributed to the superior intrinsic TC of graphene. (c) Thermal flux versus distance between flakes shown in the schematic. Each line corresponds to a simulation result with a different cross-plane TC, varying from 0.2–200 W/mK. (d) Same plot for varying flake lateral dimensions. Reprinted with permission from [71]. Copyright (2018) American Chemical Society.

heat sink junctions can be made in studies of non-curing, at least semi-fluid TIMs, despite the relative difficulty of working with them. It is common for non-curing TIMs to be out-performed by curing TIMs, all other things being held equal, including polymer base TC. Current commercial non-curing TIMs have a bulk TC range of 0.5–7 W/mK and need to reach 20–25 W/mK to allow for next-generation devices [40, 271].

Research into graphene-enhanced non-curing TIMs was up until recently exclusively studied using commercial TIMs as the matrix. These matrix materials typically start at a relatively high viscosity primarily due to having their own filler materials already incorporated, leaving little practical headroom in which one may add additional fillers. In spite of this, the addition of small quantities of graphene into these materials has shown impressive TC improvements [69, 74, 75, 272]. The presence of the commercial TIMs' undisclosed filler materials makes a detailed analysis of the observed behavior difficult.

Naghibi *et al* worked on a graphene-based non-curing TIM with a simple mineral oil base matrix for both greater insight into material properties and more room with respect to viscosity to further load with graphene [65]. The $\approx 15 \mu\text{m}$ lateral dimension graphene was mixed in with the mineral oil in addition to acetone to prevent agglomeration [273, 274]. After mixing, the acetone was removed from the mixture by

exposure to 70°C for $\approx 2 \text{ h}$ in a furnace. It was suspected that the incorporation of acetone in the mixing process helped preserve the filler quality.

Using the popular ASTM D5470 steady-state technique, the junction thermal resistance and TCs of these composites were characterized between two parallel plates. The thermal resistances of the composites between the two plates at different distances and composite concentrations are shown in figure 8(a). The inverse of the slope for every fitted line for each composite corresponds to its TC. The y-intercept of this fitted line is the sum of R_{C1} and R_{C2} from equation (1), which are equivalent to one another given the top and bottom junctions were identical. The reduction of the slope of the composites' fitted lines with increasing graphene content indicates the steady increase of bulk TC for increasing filler loadings. As previously discussed, the increasing importance of TIM TC in real-world BLTs of $300 \mu\text{m}$ is clearly presented by these findings.

Using the inverses of slopes from figures 8(a), (b) shows the derived TCs of the tested composites. The error bars convey the errors from linear regression. A sharp increase of TC, from 0.3 to 1.2 W/mK, can be seen after applying a relatively low loading of 1.9 vol.%, indicating an early onset of thermal percolation, followed by the beginning of saturation behavior at 8.5 vol.%. This behavior is well matched with a power scaling law, $K_{TIM} = A(\phi - \phi_{th})^p$, where A is a

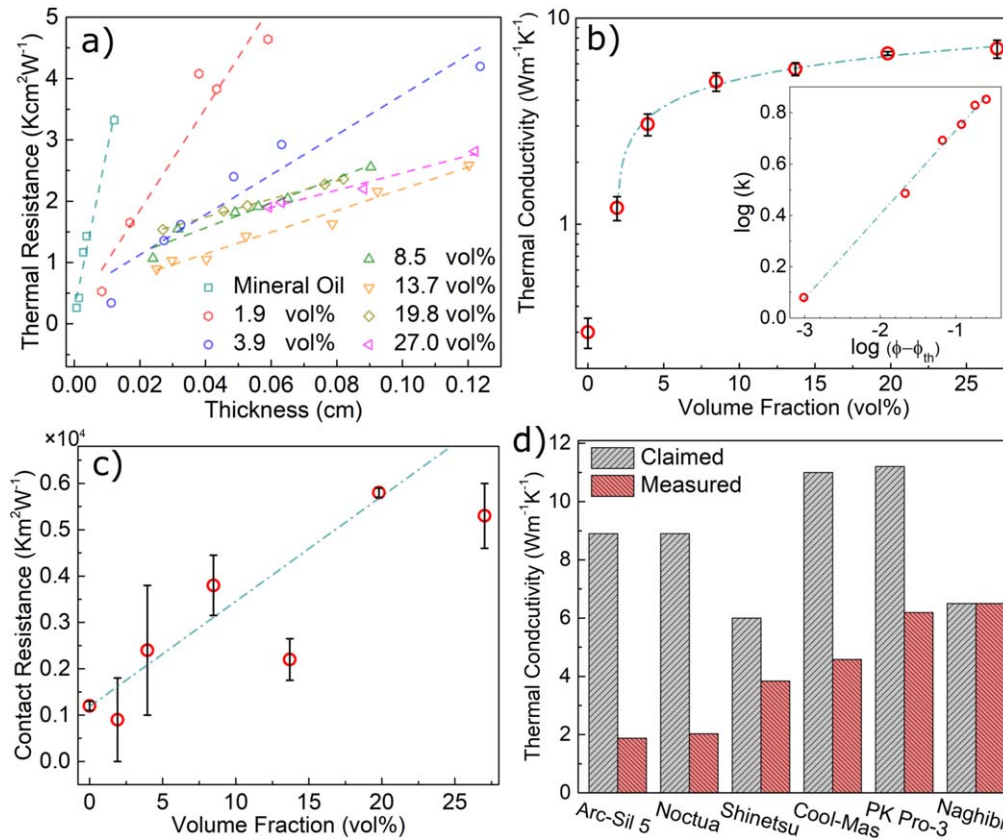


Figure 8. (a) Thermal resistance per unit area versus BLT. (b) TC as a function of volume fraction determined from the inverse of the slopes in a. (c) Contact resistance versus volume fraction with behavior dominated by the role of viscosity relating the two parameters. (d) Comparison of graphene TIMs studied with claims of TIM vendors studied with ASTM D5470. [216] John Wiley & Sons. © 2020 WILEY-VCH Verlag GmbH & Co. KGaA, Weinheim.

fitting parameter related to the effective TC with consideration to boundary resistance, ϕ_{th} is the percolation threshold and p is the universal exponent. TC saturation in non-curing TIMs has been observed previously, although it is generally absent in works looking into curing composites [275–277]. The saturation of TC is attributed to an increase of filler interface resistance as the concentration of graphene increases as a specific interaction between the filler and this individual polymer matrix [278].

Figure 8(c) shows the contact resistance of the tested composites, with increasing contact resistance for increasing loading fraction. Assuming the bulk TC of the composite is negligible in comparison to that of the mating faces in the junction, the contact resistance can be described by the following semi-empirical model:

$$R_{C_1+C_2}'' = 2R_C'' = c \left(\frac{\zeta}{k_{TIM}} \right) \left(\frac{G}{P} \right)^n, \quad (5)$$

where $G = \sqrt{G'^2 + G''^2}$. G' and G'' are the storage and loss modulus of the TIMs, P is the applied atmospheric pressure in this case, ζ is the average roughness of the two identical surfaces, and c and n are empirical coefficients [275]. Predicting the thermal contact resistance with any accuracy from successive experiments at constant pressure is challenging given that the two remaining parameters— k_{TIM} and G —are affected by graphene loading and oppose one another in the

determination of R_C'' . This equation exposes that in TIMs well described by it there is an optimum filler loading in which k_{TIM} may be substantially enhanced with little increase in R_C'' .

The bulk TC of the present 19.8 vol.% graphene TIM is compared with high-end commercial TIM products in figure 8(d). Industry self-reports TCs higher than 11 w/mK but does not disclose the technique used to arrive at those values. Here, we present all of the TIM TCs measured with the ASTM D5470 technique compared with the values reported by the manufacturers. The 19.8 vol.% graphene TIM performs better than all tested commercial TIMs. The closest performing TIM—PK Pro-3—uses ≈ 90 wt.% of aluminum and zinc oxide fillers, more than twice the loading level of the compared graphene TIM.

These TIMs have been applied to solar cells to study the reduction of performance that results from operating at elevated temperatures [13]. The poorer performance appears as a decrease in the voltage across the cell's two terminals. For every increase in operating temperature in degrees Celsius above 40 °C there is an efficiency loss of 0.35%–0.5% [279, 280]. Silicon-based solar cells are known to reach temperatures up to 65 °C, corresponding to up to a 12.5% decrease in efficiency.

It is common practice in solar cell research to analyze its performance under simulated sunlight and at greater-than-natural illumination for among other reasons, to provide the

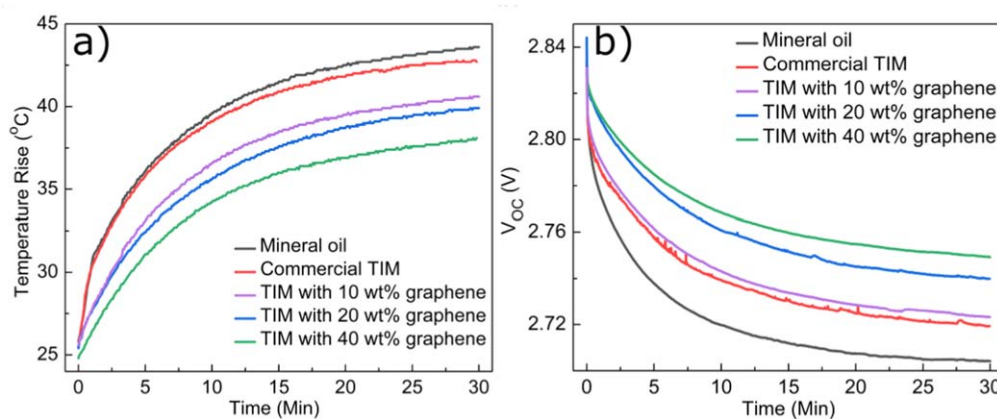


Figure 9. (a) Temperature of a solar cell over time under 70x natural solar illumination with different TIMs applied between it and a heat sink. (b) Corresponding open-circuit voltage of the solar cell that results from the device temperature. Reproduced from [13]. CC BY 3.0.

heat to elevate the device in testing above RT [281, 282]. In Mahadevan *et al.*'s work, a solar cell was fixed to a heat sink with different TIMs applied between and was illuminated with 70x and 200x natural solar illumination levels, with the former case being considered at present. Figure 9(a) shows the temperature change of a solar cell over time with different TIMs. It is evident that when the solar cell had the higher graphene concentration TIMs, the temperature that it reached remained lower, showing a better thermal coupling to its heat sink. Figure 9(b) shows the corresponding open-circuit voltages—a common photovoltaic metric of efficiency—that displays the increased efficiency gained for maintaining a lower operating temperature.

5. Hybridization and control of EC

Researchers have long noted a beneficial TC performance of composites that employ multiple types of fillers, a filling strategy known as hybridization or binary, tertiary, etc filling [47, 85, 129, 141, 147, 283–289]. This synergistic effect can be seen when including multiple filler materials at a certain constituent ratio can achieve a greater TC enhancement than with either individual filler at identical overall loading level. This effect arises from the differing morphology of the two filler materials and how they can aid one another. Despite the phenomenal intrinsic TC of graphene, which one could reasonably expect to overpower any potential synergistic effect, it has been widely reported in graphene composites [74, 118, 144, 290, 291]. This benefit occurs due to a second filler's ability to prevent graphene agglomeration in a composite and its ability to bridge gaps between graphene flakes that would otherwise force heat transport through the resistive polymer.

Due to the desire for high TC but low EC TIMs, hybridization is a promising way to leverage the extremely high TC graphene fillers while controlling the resulting composite EC that they cause. It was shown previously by Shtein *et al.* that a hybrid composite of very disparate geometries of graphene flakes and boron nitride nanoparticles could achieve synergy and a suppression of composite EC [113]. In this

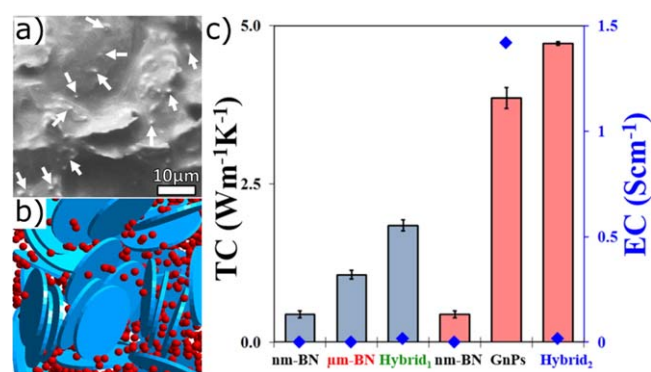


Figure 10. (a) Schematic showing mixed graphene flakes and smaller boron nitride particles. (b) SEM image of an epoxy composite with arrows pointing out boron nitride particles. (c) Plot of TC and EC of composites with total filler loading composed of 17 vol.%. 'nm-BN' corresponds to composites filled with boron nitride of 200 nm in lateral dimensions. 'μm-BN' corresponds to composites of boron nitride of approximately 40 microns. 'Hybrid 1' is 15 vol.% of μm-BN and 2 vol.% of nm-BN. 'Hybrid 2' is 16 vol.% of GnPs and 1 vol.% of nm-BN. Note the increase of TC relative to the composite of pure GnPs, which is certainly a result of synergy, as well as the sharp reduction of EC. Reprinted with permission from [72]. Copyright (2015) American Chemical Society.

work, the electrically conductive graphene flakes were effectively isolated from one another by the smaller electrically insulating boron nitride materials fitting between them, allowing thermal but not electrical conduction. This can be seen in figures 10(a) and (b), which show an SEM image and a schematic showing smaller, red boron nitride fitting between blue graphene flakes. The superiority of the composites' TC with a hybridization of filler material along with a reduction in EC can be seen in figure 10(c).

Lewis *et al.* prepared hybrid composites of graphene and *h*-BN flakes of similar geometries to investigate both whether one can achieve a more finely-tuned control on EC and as a contrapositive verification of the role that dissimilar filler geometries have in producing a synergistic effect [77]. Figure 11(a) shows a schematic of the use of hybrid fillers to selectively control composite EC while preserving useful TC. The graphene and *h*-BN flakes used both had thicknesses up

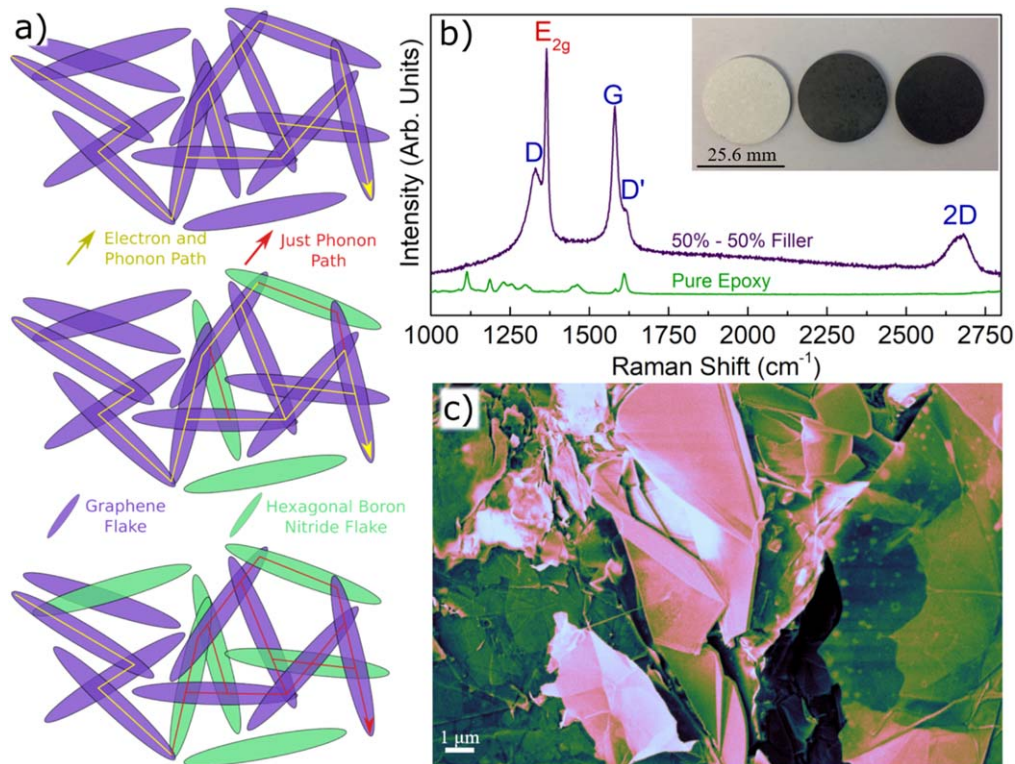


Figure 11. (a) Raman spectrum of half graphene and half *h*-BN composite with total loading of 44 vol.%. (b) Pseudo-colored SEM image of a fractured surface of a 13 vol.% of graphene and *h*-BN per composite. (c) Top schematic shows a pure graphene composite in which electrons and phonons freely move throughout. Middle schematic shows some boron nitride flakes of similar geometries thrown in, which create paths that only easily transmit phonons, but not electrons, reducing overall composite EC. Bottom schematic shows a concentration of boron nitride flakes where entire electrical percolation networks have been disrupted. Reproduced from [190]. © IOP Publishing Ltd. All rights reserved.

to 12 nm and lateral dimensions up to 8 μm . It was hypothesized that if the two materials were of comparable geometries then they would be less effective at isolating one another than had been observed previously.

Figure 11(b) shows Raman signatures of a 44 vol.% composite with 50% constituent fraction of graphene and 50% of *h*-BN (equal parts graphene and *h*-BN by volume). Characteristic peaks of graphene are present as well as the E_{2g} peak of *h*-BN [292–295]. The inset image shows selected high-loading samples. Figure 11(c) shows a pseudo-colored fractured surface of composite with pink, electrically charging *h*-BN flakes dispersed among green and blue electrically conducting graphene flakes. This image shows one instance in which neighboring graphene flakes are isolated by *h*-BN.

These composites' thermal diffusivities were measured using the common laser flash analysis (LFA) technique [296, 297]. Using densities determined from Archimedes' principle and heat capacity calculated from the Kopp–Neumann rule, the TC is calculated from the classic relation $K = \alpha \times \rho \times c_p$, where α is the thermal diffusivity, ρ is the volumetric mass density and c_p is the specific heat capacity. The LFA technique directly measures α , but combining LFA with techniques to determine the other material parameters is an exceedingly popular TC measurement strategy. The heat capacity was calculated using 0.807 J/gK for *h*-BN and 0.72 J/gK for graphite, which only notably deviates from

graphene to the ZA phonon dispersion in graphite whose states can be unfilled below 100 K [298–302].

Figure 12(a) displays the TC of color-coded composites of 11.4 vol.%, 18.1 vol.%, 25.5 vol.% and 43.6 vol.%. In all instances, as the total filler level is increased the overall TC is enhanced relative to that constituent fraction at a lower total loading. In addition, as the constituent fraction of the composites moves to higher levels of graphene (left to right on the x axis), the TC is uniformly enhanced. This result shows that a synergistic enhancement was not observed in these composites. In all tested composites, the superiority of graphene to that of *h*-BN remained the dominant factor. This provides contrapositive verification of the attribution of synergy to dissimilar filler geometries. The increased data scatter in the 25.5 vol.% is ascribed to that filler loading percentage's proximity to the percolation threshold in composites of this matrix and filler geometry [66]. This would result in some composites stochastically achieving better percolation networks than others, whereas composites above or below this loading are either firmly within or outside of a percolative filling regime. The asymmetric error bar on the 100% graphene sample at 43.6 vol.% is attributed to a clear error in the measurement of that sample's density that results from surface bubble formation.

The cross-plane ECs of the composites were measured by simply painting silver electrodes on opposing faces of the samples and measuring the resistance from the two-probe

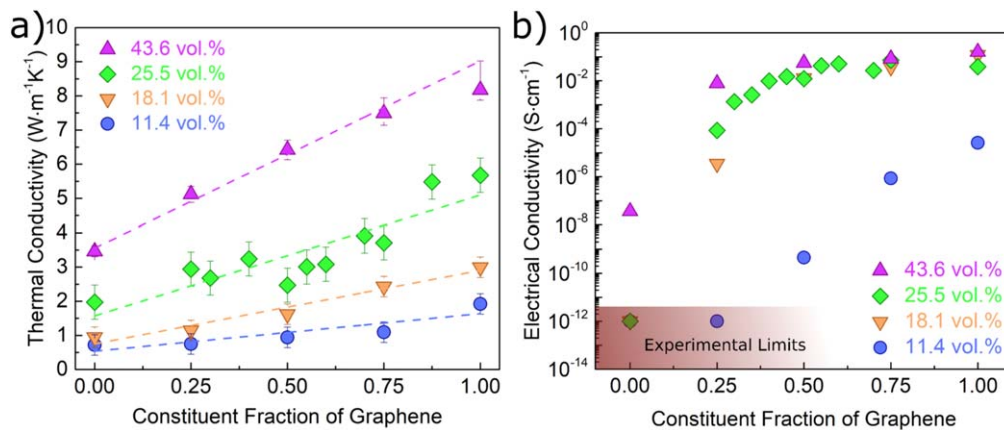


Figure 12. (a) TC of each set of total filler level versus the graphene/*h*-BN constituent ratio. Data points at 1.00 on the *x* axis correspond to a sample at the stated vol.% composed of only graphene and matrix. (b) EC of the studied composites displaying a power scaling law. Reproduced from [190]. © IOP Publishing Ltd. All rights reserved.

method in a process that has been used in similar studies [303, 304]. This method allowed for easier determination of *cross-plane* EC than the 4-probe or van der Pauw methods could provide given the geometry of the samples. Figure 12(b) shows the EC in the same manner as figure 12(a) with the constituent fraction of graphene on the *x* axis. The obtained EC results show a range of at least 11 orders of magnitude, though the full range is obscured due to experimental limitations. For all total filler levels, a strong dependence on the constituent fraction of graphene is observed with a power-law dependence. At total filler level greater than 11.4 vol.% the composites' ECs saturate at constituent graphene level of 25%.

Another work by Cui *et al* on composites with similar materials of different shapes, sheets of *h*-BN of ≈ 250 nm and sheets of graphene of ≈ 5 μm in lateral size, noted TC synergy [118]. The authors achieved a TC of 1.31 W/mK in polyamide with 20 wt.% graphene compared to 0.28 W/mK in pure polyamide. When the authors included a mere 1.5 wt.% in addition to the graphene, they achieved a TC of 1.76 W/mK. It very likely that this marked enhancement relative to the previous sample with only graphene is due to synergistic enhancement of the two fillers. It is true that in these composites the overall filler loading is increased and could be approaching the percolation regime of thermal performance, though this observed percolation threshold is lower than where others have found it.

Hybrid composites have been interestingly investigated with graphene and alumina spheres of multiple diameters (5 and 0.7 μm), effectively using three loading materials in a silicone oil matrix [305]. The different size alumina fillers are varied as a parameter to achieve higher packing density at the expense of larger fillers to allow larger unobstructed thermal pathways [306]. In a composite only composed of the two alumina sphere sizes, an optimal synergistic ratio of 15 vol.% of smaller alumina and 45 vol.% of larger alumina was observed. This parametric optimization between the concentrations of two filler types is the defining characteristic of the synergy mechanism. Raising the total concentration at fixed constituent ratio of the alumina composite from

60 vol.% to 63 vol.% results in an increase of 0.49 W/mK, and adding just 1 wt.% of graphene results in a further 0.75 W/mK improvement up to a total of ≈ 3.5 W/mK. Similarly, Guan *et al* found that epoxy filled with 80 wt.% had a TC of 0.8 W/mK while substituting the last 7 wt.% for graphene achieved a TC of 1.8 W/mK [307].

Barani *et al* published a study of graphene and copper nanoparticle hybrid-filled TIMs that exhibited likely synergistic thermal properties [121]. This work used graphene with lateral dimensions of ≈ 25 μm and copper spheres with diameters of 40, 100, and 580 nm. Given the copper nanoparticles' conformance to the Wiedemann–Franz Law, it is vitally important to preserve the EC of the material to, in turn, preserve the TC. To that end, the smallest copper nanoparticle size corresponded to roughly the electron mean free path in copper. Generally, the mean free paths of whatever dominant heat carrier of a considered filler material is a crucial consideration in the minimum size that can still effectively transport heat. In the case of copper nanoparticle fillers, extraordinary care must be taken to prevent rapid and unsafe oxidation that can reduce the TC by an order of magnitude [308]. Figure 13(a) shows the thermal diffusivity of 5 wt.%, 15 wt.%, and 40 wt.% graphene TIMs with increasing copper loading as binary TIMs. As expected, the composites that contain a higher load level of graphene fillers have a higher thermal diffusivity. Figures 13(b)–(d) show the calculated TC of each composite. Notably, in figure 13(c), a sharp increase in the TC of the 15 wt.% TIM can be seen between 35 wt.%–40 wt.%. This dramatic enhancement in TC followed by little improvement, even possibly a slight reduction, suggests that a critical optimum of constituent fraction has been reached and moving past it does not further improve performance.

6. Lifespan reliability and performance

Along with the associated costs, one of the primary reasons polymeric TIMs receive such preferential usage in industry is due to their lifespan performance versus, for instance, metallic and pad TIMs. It is perceived by the current authors to be a

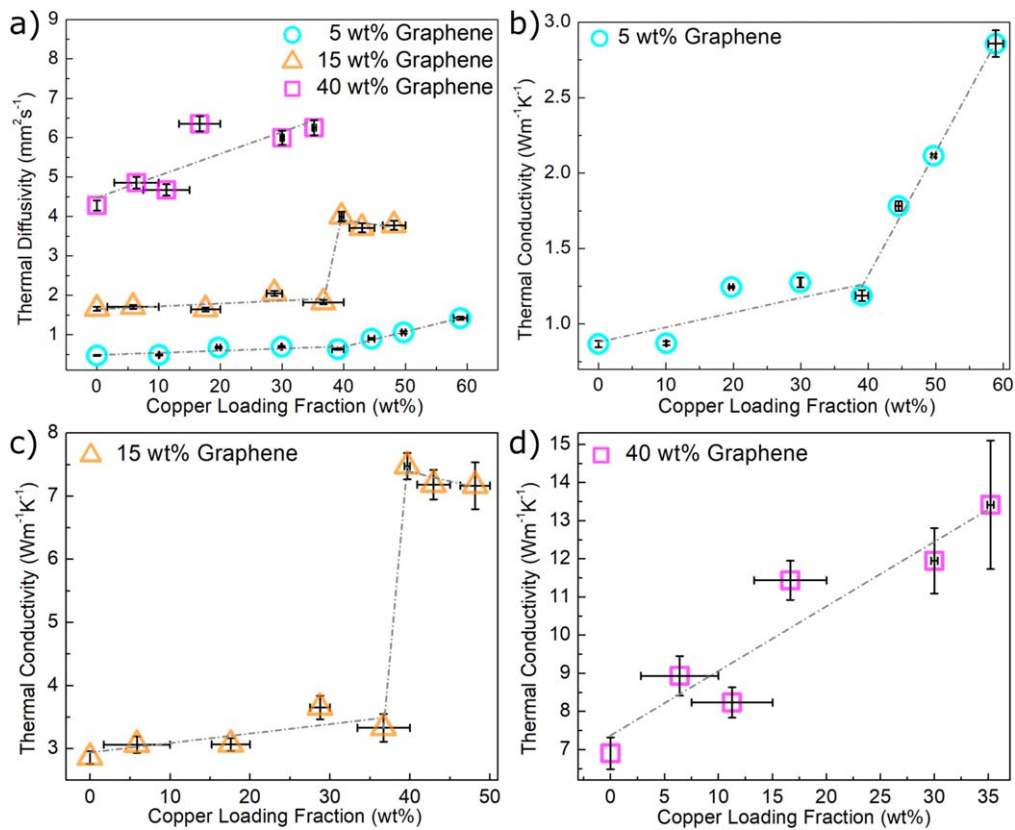


Figure 13. (a) Thermal diffusivity of 5 wt.%, 15 wt.%, and 40 wt.% graphene TIMs with increasing copper loading as binary TIMs. Subfigures (b), (c) and (d) are TCs calculated for each graphene concentration plotted in subfigure (a). [114] John Wiley & Sons. © 2019 WILEY-VCH Verlag GmbH & Co. KGaA, Weinheim.

short-coming of TIM research that lifespan performance of novel TIMs is so seldom considered, especially in graphene-based TIMs, likely borne from the time commitment such a study would entail. TIMs are by their very nature applied in very difficult environments and need to maintain performance for as long as possible, very often for the entire lifespan of the device. As the devices are turned on and off, operated in humid environments, and exposed to environmental contaminants, their intrinsic material characteristics can alter as well as the morphology of the mating surface in which they are applied. Each of these alterations can lead to catastrophic failure from cracking or being pumped out of the junction as a result of the thermal expansion, contraction and warping over the course of high- and low-power device state fluctuations. Perhaps the largest factor affecting the lifespan performance of TIM in-junction is the coefficient of thermal expansion mismatches between the TIM and junction. The problems that can arise can take the form of cracks, voids, or intrinsic denaturing of the TIM. Figures 14(a)–(c) show acoustic microscopy images of a TIM application that is still intact, exhibits voids and has cracks [309]. Figures 14(d)–(f) show corresponding infrared thermography images a few milliseconds after powering the device, which shows faster heat spread on the TIM with superior coverage.

Although the fraction of published works that report lifespan performance to total works published on polymeric TIMs is quite low, researchers have considered this often

overlooked aspect [115, 309–311]. The literature on this matter, unfortunately, is quite inconsistent likely due to the lack of a universal standard technique for reliability and the likelihood that any developed standard technique would be unable to provide predictive performance for every individual device application. There are three classes of accelerated aging techniques within which most of the experiments conducted into TIM reliability can be categorized: elevated temperature storage, temperature cycling, and power cycling [310].

Elevated temperature storage procedures hold a TIM typically in a junction sandwich at a uniform elevated temperature for an extended period of time. Very importantly, they may or may not employ a high humidity environment to simulate important moisture interactions. The performance of TIMs in this test varies greatly depending on the TIM and junction materials, showing both enhanced and hindered performance over the course of treatment [312–319]. Likewise, a TIM can either experience enhancement from humidity that results from increased wetting or experience impairment of the adhesion ability of the polymer matrix [313, 320]. The lack of consistency in this type of procedure has numerous causes from differences in the procedure, different materials, chemical degradation, and physical form changes.

More representative of realistic TIM conditions is the temperature cycling procedure. In this technique, the TIMs

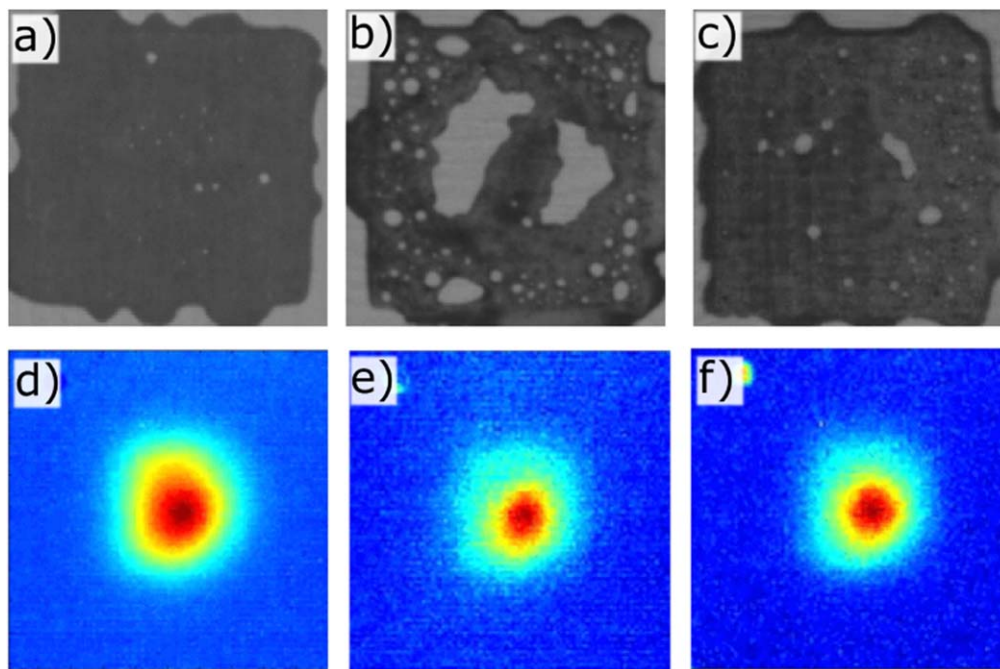


Figure 14. Top rows are scanning acoustic microscope and bottom are IR thermography images taken a few milliseconds after device powering on. (a) High-quality TIM application, (b) TIM application with substantial voids, and (c) TIM application with micro-cracks. (d), (e) and (f) are IR thermography images corresponding to (a), (b) and (c), respectively. Quicker spread of temperature in (d) than (e) and (f), evidenced by the wider red and green region, demonstrates a quicker heat spread than the other two samples. © 2006 IEEE. Reprinted, with permission, from [259].

often inside an overall junction are cyclically placed in uniform high- and low-temperature environments. This procedure more closely approximates real-world TIM conditions because of the fact that TIMs operate at a wide range of temperatures. This procedure allows for multiple thermal expansions and contractions to occur, which is an important parameter in TIM pump-out and cracking. The results in the literature for this procedure are inconsistent as well, with most non-curing TIMs performing better [316, 319, 321]. It was observed previously that most of these instances of improvement were attributed to a reduction of the BLT and increased wetting, with each mechanism not being a contributing factor to cured TIMs [310].

Likely the most representative accelerated aging method is power cycling. In this technique, a TIM often with its accompanying junction are cyclically heated from a localized source, resulting in a temperature gradient. This method captures thermal expansion and contraction mechanisms experienced in TIM applications the closest. Non-curing TIMs typically exhibit a reduction in performance between 20%–60%, showing the superiority of this technique in reproducing real-world behavior [310]. Because the sample is being heated from one side, it is of greater importance that one considers the rate of heating. If the heat were too high in the localized spot where the heater is located, then it would increase the effective thermal expansion mismatch in either just the TIM or the entire TIM and junction sandwich.

Lewis *et al* worked on a power-cycled reliability study on graphene-filled epoxy TIMs, without an adjoining junction [322]. The decision to not examine the TIM inside a junction

sandwich stemmed from a desire to analyze the intrinsic TC lifespan performance and to simplify the procedure for reproducibility. A custom Nichrome wire heating loop between Kapton was fabricated to be used as the localized heating element. As part of a control system, a Type-J thermocouple was fixed to the back of the sample as a feedback to inform us how much electrical power we need to supply to the heating coil. In the Python programming language, a calibration algorithm determined the amount of power that was needed to supply to the coil to achieve the desired temperature range without any assumptions of material properties. It then ran unattended with intermittent re-calibration events. Figure 15 shows a schematic of the power cycle treatment procedure. In addition, a small electronic fan was programmatically controlled to speed the cooling phase of the power cycle.

At specified power cycle counts, samples were removed from the power cycling apparatus and experimented with LFA to directly measure their thermal diffusivity. Figures 16(a) and (b) show the thermal diffusivities and conductivities for pure epoxy, while figures 16(c) and (d) show that of 5.4 vol.%, and figures 16(e) and (f) show that of 30 vol.% samples. For all samples and at all power cycle counts, the thermal diffusivity reduced with increasing temperature. The initial RT diffusivities were 0.17, 1.25, and 4.6 mm²s⁻¹, in order of increasing load level. After each sample's cycling treatments, their RT thermal diffusivities reached 0.17, 1.57, and 5.40 mm²s⁻¹, in the same order, corresponding to a cycled percent enhancement of 0%, 25.6%, and 17.4%. Interestingly, a clear increase in thermal

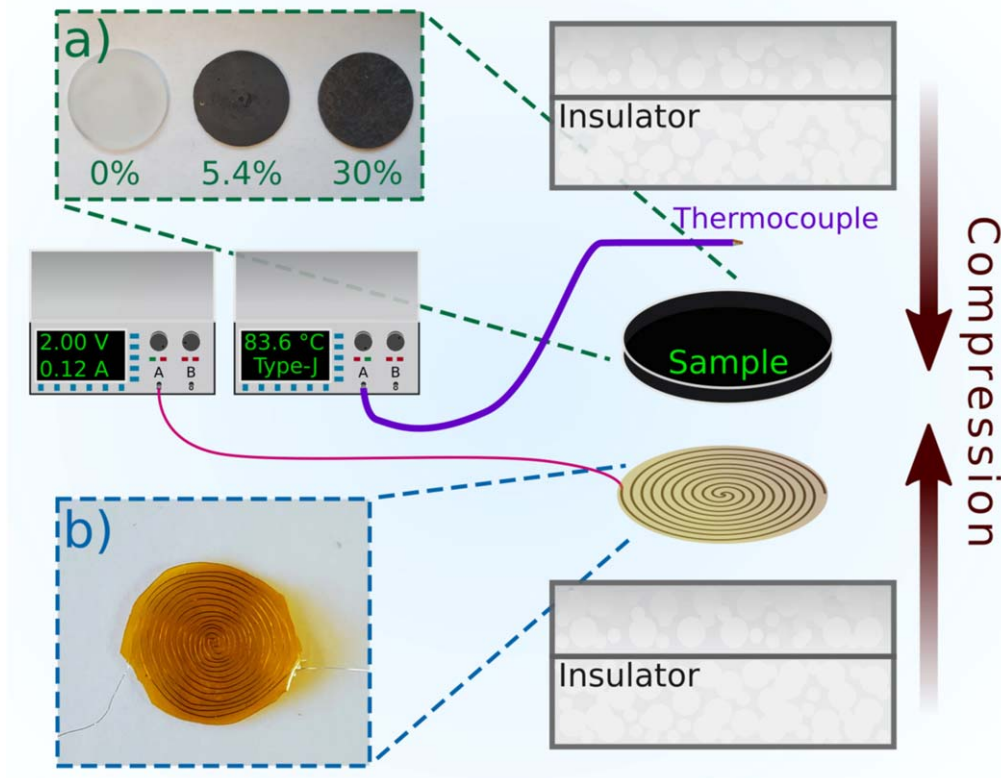


Figure 15. Schematic of the power cycling procedure. Power supply passes current through a custom wire coil heater and a thermocouple on the back side of the sample and measures the corresponding equilibrium temperature for that power level. Insulators, thermocouple, sample and heating coil were all fixed in position with light compression. (a) Image of the sample pre-treatment and (b) an image of an example heating coil. Reproduced from [272]. CC BY 4.0.

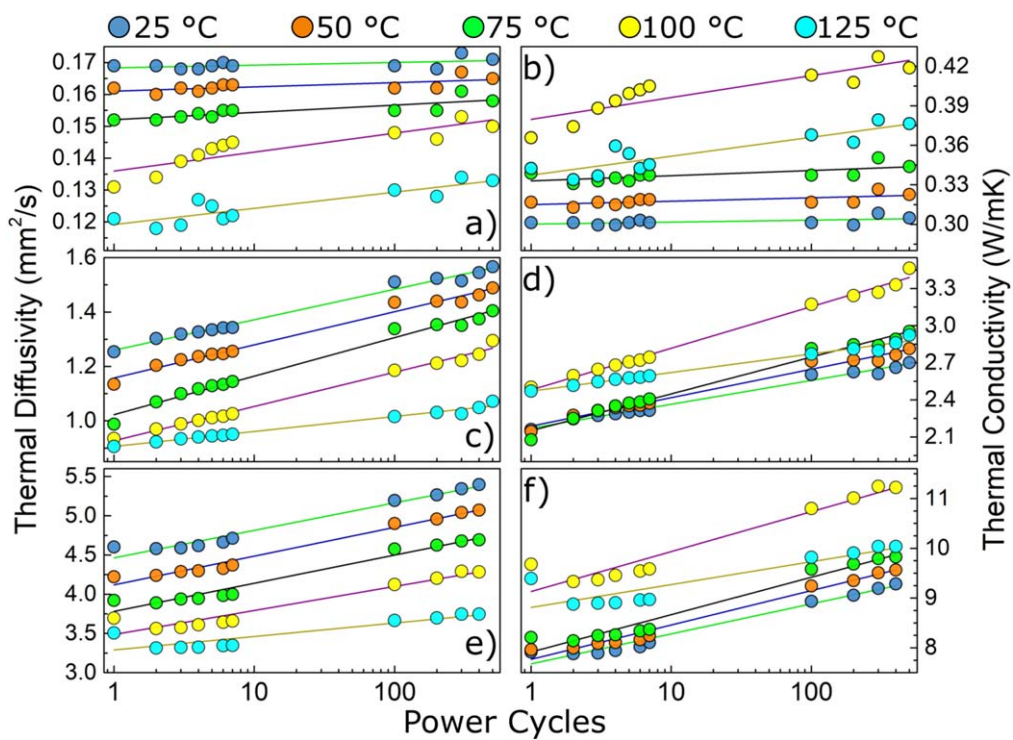


Figure 16. Panels on the left show thermal diffusivity and panels on the right show TC. (a) Pure epoxy samples, (b) 5.4 vol.% samples and (c) 30 vol.% samples. Reproduced from [272]. CC BY 4.0.

diffusivity can be seen in loaded samples over the course of cycling. Although the pure epoxy sample does show modest improvement over the course of its cycling, it can only be seen at elevated temperatures, whereas the loaded samples show a more marked improvement at lower temperatures.

Using the classic definition of TC, $K = \alpha\rho C_p$, LFA experiments for α , Archimedes' principle experiments for ρ , and Kopp–Neumann rule for C_p , the TCs of the composites were determined. After power cycling, the 30 vol.% sample achieved a TC of 9.3 W/mK at RT, placing the sample among the highest reported for graphene-enhanced TIMs at this loading level [66, 102]. The pure epoxy sample did experience TC enhancement only past 100 °C, with a modest enhancement of 7.7% at that temperature, from 0.39 to ≈ 0.42 W/mK. However, the 5.4 vol.% and 30 vol.% samples each improved substantially over the course of cycling, constituting an improvement of 24.9% and 17.3%, respectively. The tendency for the TC of each composite to increase with temperature is primarily dictated by the composite's heat capacity behavior as the temperature is varied.

In each sample and at all cycle counts, the TC at 125 °C is lower than at 100 °C. This is attributed to the fact that the glass transition temperature of this material is at around 100 °C and thermal properties are known to degrade in polymers beyond this temperature [112, 323, 324]. It has been reported previously that polymer glass transitions can be elevated with volumetric substitution of inert materials, such as graphene [325, 326]. The appearance of a reduction in performance at 125 °C indicates that any elevation of glass transition point must be less than 25 °C in total. An increase of 30 °C was seen previously in a PMMA polymer matrix with the inclusion of functionalized graphene. This suggests that graphene does not greatly inhibit the epoxy's cross-linking.

No sample's performance decreased over the entire course of power cycling treatments. At low temperature, the pure epoxy sample's TC performance remained largely unchanged. Interestingly, the samples loaded with graphene, 5.4 vol.% and 30 vol.%, showed a consistent increase in performance over the course of treatment. Due to the elimination of junction alterations as a factor to influence the TIM performance, the obtained results effectively present the intrinsic lifespan behavior of graphene TIMs, which should be more reproducible due to the simplified experiment. Should this study have been conducted in a junction it is very possible that the performance over the course of treatment would have decreased, as happened previously in a lifespan study of silver-filled epoxies [327].

Khuu *et al* conducted accelerated lifespan research into a pure epoxy TIM that showed modest thermal resistance reductions of 8%, suggested to be caused by increasing the level of epoxy cross-linking [317]. Lewis *et al*'s study on pure epoxy is mostly in agreement with the previous results with only modest increases in TC—which would provide for a reduction in observed thermal resistance—and negligible difference at temperatures below 100 °C. When graphene is added to the epoxy, however, a clear increase in TC at all temperatures is observed over the course of power cycling,

amounting to an enhancement of 24.9% in 5.4 vol.% and 17.3% in 30 vol.%. Clearly from these results, graphene must play an essential role in the intrinsic TIM performance over the course of accelerated aging.

It was reasoned that the increased cross-linking mechanism for enhanced performance proposed earlier could explain the large increase in graphene-epoxy TIMs but only modest increase in pure epoxy TIMs. If the epoxy matrix is increasing its level of cross-linking, then it is swelling and simultaneously getting more and more rigid, leading to tighter mechanical coupling between the graphene and epoxy matrix [323]. This would lead to a lower Kapitza resistance between the two materials. As polymers are elevated in temperature the cross-linking rate can increase and once that reaction has taken place, it is irreversible with respect to temperature. This can explain why over the course of power cycling the performance improves and why the improvement occurs even when tested at RT.

7. Outlook

TIMs play an important and increasing role in the behavior of high-power electronic circuits and VLSI chips. Device miniaturization and densification are driving the unceasing demand for ever-improving TIM performance. Cost of production, ease of application, safety around exposed circuit elements, and lifespan reliability all contribute to the wide-scale adoption of polymer-based TIMs in industry. In order to improve the performance of polymer matrix TIMs, microscopic fillers of very high TC are dispersed within them. Due to graphene's phenomenal intrinsic TC and its advantageous quasi-2D geometry, there is substantial research into it as a filler material. Graphene's thermal coupling to the polymer matrix in which it is dispersed as well as its dispersibility can be further enhanced by functionalizing the graphene with other materials. Tremendous potential for extraordinary TC enhancement exists for the effective and facile alignment of graphene fillers.

Increasing the load level of graphene in TIMs results in a superlinear TC enhancement past a point known as the thermal percolation threshold. The highest-performance graphene TIMs are prepared at concentrations beyond this load level. Special consideration will need to be given to these highly loaded composites' viscosity and workability. In this percolative loading regime, graphene's cross-plane TC plays a large role as the weakest link in the overall heat flow.

Many TIM applications are very sensitive to its EC, whether the TIM directly encapsulates or is at risk of spilling onto active circuits due to junction pump-out as the device—typically VLSI chip—alternates between high- and low-power states. Because graphene has a high EC as well as TC, special care with electrically sensitive applications must be taken to either not surpass the electrical percolation threshold or to use a clever hybrid filler strategy to disrupt otherwise formed electrical networks within the composite.

TIMs by their nature must operate over a realistic lifespan. Any promising TIM developments require a full

lifespan analysis before its industrial efficacy can be fully assessed. Unfortunately, there is little consistency among studies that are concerned with lifespan performance. It is recommended by the authors that a more simplified approach to TIM accelerated aging be taken, hopefully to achieve more consistency and reproducibility in this research by reducing the number of testing parameters.

ORCID iDs

Jacob S Lewis  <https://orcid.org/0000-0002-5452-2045>
 Timothy Perrier  <https://orcid.org/0000-0003-4996-4233>
 Fariborz Kargar  <https://orcid.org/0000-0003-2192-2023>
 Alexander A Balandin  <https://orcid.org/0000-0002-9944-7894>

References

- [1] Thompson S E and Parthasarathy S 2006 Moore's law: the future of Si microelectronics *Mater. Today* **9** 20–5
- [2] Krishnan S, Garimella S V, Chrysler G M and Mahajan R V 2007 Towards a thermal Moore's law *IEEE Trans. Adv. Packag.* **30** 462–74
- [3] Lin S and Banerjee K 2008 Cool chips: opportunities and implications for power and thermal management *IEEE Trans. Electron Devices* **55** 245–55
- [4] Yu Z, Wang R, Hao P, Guo S, Ren P and Huang R 2018 Non-universal temperature dependence of hot carrier degradation (HCD) in finFET: New observations and physical understandings 2018 *IEEE Electron Devices Technology and Manufacturing Conf., EDTM 2018—Proc. (Kobe, Japan)* (Institute of Electrical and Electronics Engineers Inc.) pp 34–6
- [5] Guo A and Del Alamo J A 2017 Unified mechanism for positive- and negative-bias temperature instability in GaN MOSFETs *IEEE Trans. Electron Devices* **64** 2142–7
- [6] Bury E, Chasin A, Kaczer B, Chuang K H, Franco J, Simicic M, Weckx P and Linten D 2018 Self-heating-aware CMOS reliability characterization using degradation maps *IEEE International Reliability Physics Symposium Proc. (Burlingame, CA)* (Institute of Electrical and Electronics Engineers Inc.) **2A.31–6**
- [7] Arik M and Weaver S 2004 Chip-scale thermal management of high-brightness LED packages *Fourth International Conf. on Solid State Lighting* vol 5530 ed I T Ferguson et al (International Society for Optics and Photonics, SPIE) pp 214–23
- [8] Tang Y, Liu D, Yang H and Yang P 2016 Thermal effects on LED lamp with different thermal interface materials *IEEE Trans. Electron Devices* **63** 4819–24
- [9] Cho E-C, Huang J-H, Li C-P, Chang-Jian C-W, Lee K-C, Hsiao Y-S and Huang J-H 2016 Graphene-based thermoplastic composites and their application for LED thermal management *Carbon* **102** 66–73
- [10] Zhang H, Lin Y, Zhang D, Wang W, Xing Y, Lin J, Hong H and Li C 2016 Graphene nanosheet/silicone composite with enhanced thermal conductivity and its application in heat dissipation of high-power light-emitting diodes *Curr. Appl. Phys.* **16** 1695–702
- [11] Saadah M, Hernandez E and Balandin A 2017 Thermal management of concentrated multi-junction solar cells with Graphene-Enhanced thermal interface materials *Appl. Sci.* **7** 589
- [12] Barako M T, Gambin V and Tice J 2018 Integrated nanomaterials for extreme thermal management: a perspective for aerospace applications *Nanotechnology* **29** 154003
- [13] Mahadevan B K, Naghibi S, Kargar F and Balandin A A 2019 Non-curing thermal interface materials with graphene fillers for thermal management of concentrated photovoltaic solar cells *C—Journal of Carbon Research* **6** 2
- [14] Song N, Cao D, Luo X, Wang Q, Ding P and Shi L 2020 Highly thermally conductive polypropylene/graphene composites for thermal management *Composites A* **135** 105912
- [15] Lorenzini D and Joshi Y 2019 Flow boiling heat transfer in silicon microgaps with multiple hotspots and variable pin fin clustering *Phys. Fluids* **31** 102002
- [16] Kang S-W, Wei W-C, Tsai S-H and Yang S-Y 2006 Experimental investigation of silver nano-fluid on heat pipe thermal performance *Appl. Therm. Eng.* **26** 2377–82
- [17] Boukhanouf R, Haddad A, North M T and Buffone C 2006 Experimental investigation of a flat plate heat pipe performance using IR thermal imaging camera *Appl. Therm. Eng.* **26** 2148–56
- [18] Greenwood J A and Williamson J B P 1966 Contact of nominally flat surfaces *Proc. of the Royal Society of London. Series A. Mathematical and Physical Sciences* **295** 300–19
- [19] Jones M H, Howells R I L and Probert S D 1968 Solids in static contact *Wear* **12** 225–40
- [20] Cooper M G, Mikic B B and Yovanovich M M 1969 Thermal contact conductance *Int. J. Heat Mass Transfer* **12** 279–300
- [21] Burger N, Laachachi A, Ferriol M, Lutz M, Toniazio V and Ruch D 2016 Review of thermal conductivity in composites: Mechanisms, parameters and theory *Prog. Polym. Sci.* **61** 1–28
- [22] Prasher R S 2001 Surface chemistry and characteristics based model for the thermal contact resistance of fluidic interstitial thermal interface materials *J. Heat Transfer* **123** 969–75
- [23] Sarvar F, Whalley D C and Conway P P 2006 Thermal interface materials—A review of the state of the art *ESTC 2006-1st Electronics Systemintegration Technology Conf. vol 2* (Institute of Electrical and Electronics Engineers Inc.) pp 1292–302
- [24] Razeeb K M, Dalton E, Cross G L W and Robinson A J 2018 Present and future thermal interface materials for electronic devices *Int. Mater. Rev.* **63** 1–21
- [25] Naghibi S 2020 Noncuring graphene thermal interface materials for advanced electronics *PhD Thesis UC Riverside* (<https://escholarship.org/uc/item/708332gw>)
- [26] Chung D D L 2001 Thermal interface materials *J. Mater. Eng. Perform.* **10** 56–9
- [27] Deppisch C, Fitzgerald T, Raman A, Hua F, Zhang C, Liu P and Miller M 2006 The material optimization and reliability characterization of an indium-solder thermal interface material for CPU packaging *JOM* **58** 67–74
- [28] Gao Y and Liu J 2012 Gallium-based thermal interface material with high compliance and wettability *Appl. Phys. A: Mater. Sci. Process.* **107** 701–8
- [29] Roy C K, Bhavnani S, Hamilton M C, Johnson R W, Nguyen J L, Knight R W and Harris D K 2015 Investigation into the application of low melting temperature alloys as wet thermal interface materials *Int. J. Heat Mass Transfer* **85** 996–1002
- [30] Nagabandi N, Yegin C, Feng X, King C, Oh J K, Scholar E A, Narumanchi S and Akbulut M 2018 Chemically linked metal-matrix nanocomposites of boron nitride nanosheets and silver as thermal interface materials *Nanotechnology* **29** 105706
- [31] Macris C G, Sanderson T R, Ebel R G and Leyerle C B 2004 Performance, reliability, and approaches using a low melt alloy as a thermal interface material *Proc. IMAPS* (http://enerdynesolutions.com/downloads/imaps_2004_man.pdf)

- [32] Subramanian S J 2005 Mechanical modeling of a solder thermal interface material: Implications for thermo-mechanical reliability *Proc. of the ASME/Pacific Rim Technical Conf. and Exhibition on Integration and Packaging of MEMS, NEMS, and Electronic Systems: Advances in Electronic Packaging 2005* (American Society of Mechanical Engineers Digital Collection) pp 959–63
- [33] Otiaba K C, Okereke M I and Bhatti R S 2014 Numerical assessment of the effect of void morphology on thermo-mechanical performance of solder thermal interface material *Appl. Therm. Eng.* **64** 51–63
- [34] Too S S, Touzelbaev M, Khan M, Master R, Diep J and Keok K H 2009 Indium thermal interface material development for microprocessors *Annual IEEE Semiconductor Thermal Measurement and Management Symposium* pp 186–92
- [35] Ekpu M, Bhatti R, Okereke M I, Mallik S and Otiaba K 2014 Fatigue life of lead-free solder thermal interface materials at varying bond line thickness in microelectronics *Microelectron. Reliab.* **54** 239–44
- [36] Roy C K, Bhavnani S, Hamilton M C, Johnson R W, Knight R W and Harris D K 2016 Thermal performance of low melting temperature alloys at the interface between dissimilar materials *Appl. Therm. Eng.* **99** 72–9
- [37] Carbonaut (<https://www.thermal-grizzly.com/produkte/298-carbonaut>) Accessed: 09-03-2020.
- [38] Trew R J, Green D S and Shealy J B 2009 AlGaIn/GaN HFET reliability *IEEE Microw. Mag.* **10** 116–27
- [39] Huang X, Jiang P and Tanaka T 2011 A review of dielectric polymer composites with high thermal conductivity *IEEE Electr. Insul. Mag.* **27** 8–16
- [40] Gwinn J P and Webb R L 2003 Performance and testing of thermal interface materials *Microelectron. J.* **34** 215–22
- [41] Xu Y, Luo X and Chung D D L 1999 Sodium silicate based thermal interface material for high thermal contact conductance *J. Electron. Packag.* **122** 128–31
- [42] Guthy C, Du F, Brand S, Winey K I and Fischer J E 2007 Thermal conductivity of single-walled carbon nanotube/PMMA nanocomposites *J. Heat Transfer* **129** 1096–9
- [43] Zhou W 2011 Thermal and dielectric properties of the AlN particles reinforced linear low-density polyethylene composites *Thermochim. Acta* **512** 183–8
- [44] d'Almeida J R M, Cella N, Monteiro S N and Miranda L C M 1998 Thermal diffusivity of an epoxy system as a function of the hardener content *J. Appl. Polym. Sci.* **69** 1335–41
- [45] Wong C P and Bollampally R S 1999 Thermal conductivity, elastic modulus, and coefficient of thermal expansion of polymer composites filled with ceramic particles for electronic packaging *J. Appl. Polym. Sci.* **74** 3396–403
- [46] Murshed S M S, Leong K C and Yang C 2005 Enhanced thermal conductivity of TiO₂-water based nanofluids *Int. J. Therm. Sci.* **44** 367–73
- [47] Sim L C, Ramanan S R, Ismail H, Seetharamu K N and Goh T J 2005 Thermal characterization of Al₂O₃ and ZnO reinforced silicone rubber as thermal pads for heat dissipation purposes *Thermochim. Acta* **430** 155–65
- [48] Cola B A, Xu X and Fisher T S 2007 Increased real contact in thermal interfaces: a carbon nanotube/foil material *Appl. Phys. Lett.* **90** 093513
- [49] Zeng J, Cao Z, Yang D, Sun L and Zhang L 2009 Thermal conductivity enhancement of Ag nanowires on an organic phase change material *J. Therm. Anal. Calorim.* **101** 385–9
- [50] Yu W, Xie H, Li Y and Chen L 2011 Experimental investigation on thermal conductivity and viscosity of aluminum nitride nanofluid *Particuology* **9** 187–91
- [51] Burger N, Laachachi A, Mortazavi B, Ferriol M, Lutz M, Toniazzo V and Ruch D 2015 Alignments and network of graphite fillers to improve thermal conductivity of epoxy-based composites *Int. J. Heat Mass Transfer* **89** 505–13
- [52] Yu W, Zhao J, Wang M, Hu Y, Chen L and Xie H 2015 Thermal conductivity enhancement in thermal grease containing different CuO structures *Nanoscale Res. Lett.* **10** 1–8
- [53] Du H, Qi Y, Yu W, Yin J and Xie H 2017 T-shape ZnO whisker: a more effective thermal conductive filler than spherical particles for the thermal grease *Int. J. Heat Mass Transfer* **112** 1052–6
- [54] Quinton B, Elston L, Scofield J and Mukhopadhyay S 2018 C —*Journal of Carbon Research* **4** 28
- [55] Devananda P R and NarayanPrabhu K 2019 The effect of load and addition of MWCNTs on silicone based TIMs on thermal contact heat transfer across Cu/Cu interface *Mater. Res. Express* **6** 1165h9
- [56] Theerthagiri J, Salla S, Senthil R A, Nithyadharseni P, Madankumar A, Arunachalam P, Maiyalagan T and Kim H-S 2019 A review on ZnO nanostructured materials: energy, environmental and biological applications *Nanotechnology* **30** 392001
- [57] Sharma V, Kagdada H L, Jha P K, Spiewak P and Kurzydowski K J 2020 Thermal transport properties of boron nitride based materials: a review *Renew. Sustain. Energy Rev.* **120** 109622
- [58] Levy I, Wormser E, Varenik M, Buzaglo M, Nadiv R and Regev O 2019 Graphene-graphite hybrid epoxy composites with controllable workability for thermal management *Beilstein J. Nanotechnol.* **10** 95–104
- [59] Ohayon-Lavi A, Buzaglo M, Ligati S, Peretz-Damari S, Shachar G, Pinsk N, Riskin M, Schatzberg Y, Genish I and Regev O 2020 Compression-enhanced thermal conductivity of carbon loaded polymer composites *Carbon* **163** 333–40
- [60] Zhao Y-H, Zhang Y-F, Wu Z-K and Bai S-L 2016 Synergic enhancement of thermal properties of polymer composites by graphene foam and carbon black *Composites B* **84** 52–8
- [61] Cui T, Li Q, Xuan Y and Zhang P 2015 Preparation and thermal properties of the graphene-polyolefin adhesive composites: application in thermal interface materials *Microelectron. Reliab.* **55** 2569–74
- [62] Yu A, Ramesh P, Itkis M E, Bekyarova E and Haddon R C 2007 Graphite nanoplatelet-epoxy composite thermal interface materials *J. Phys. Chem. C* **111** 7565–9
- [63] Debelak B and Lafdi K 2007 Use of exfoliated graphite filler to enhance polymer physical properties *Carbon* **45** 1727–34
- [64] Choi S U S, Zhang Z G, Yu W, Lockwood F E and Grulke E A 2001 Anomalous thermal conductivity enhancement in nanotube suspensions *Appl. Phys. Lett.* **79** 2252–4
- [65] Naghibi S, Kargar F, Wright D, Huang C Y T, Mohammadzadeh A, Barani Z, Salgado R and Balandin A A 2020 Noncuring graphene thermal interface materials for advanced electronics *Adv. Electron. Mater.* **6** 1901303
- [66] Kargar F, Barani Z, Salgado R, Debnath B, Lewis J S, Aytan E, Lake R K and Balandin A A 2018 Thermal percolation threshold and thermal properties of composites with high loading of Graphene and Boron nitride fillers *ACS Appl. Mater. Interfaces* **10** 37555–65
- [67] Yan H, Tang Y, Long W and Li Y 2014 Enhanced thermal conductivity in polymer composites with aligned graphene nanosheets *J. Mater. Sci.* **49** 5256–64
- [68] Olowojoba G B, Eslava S, Gutierrez E S, Kinloch A J, Mattevi C, Rocha V G and Taylor A C 2016 In situ thermally reduced graphene oxide/epoxy composites: thermal and mechanical properties *Appl. Nanosci. (Switzerland)* **6** 1015–22
- [69] Goyal V and Balandin A A 2012 Thermal properties of the hybrid graphene-metal nano-micro-composites: Applications in thermal interface materials *Appl. Phys. Lett.* **100** 073113

- [70] Goli P, Legedza S, Dhar A, Salgado R, Renteria J and Balandin A A 2014 Graphene-enhanced hybrid phase change materials for thermal management of Li-ion batteries *J. Power Sources* **248** 37–43
- [71] Zhong Y, Zhou M, Huang F, Lin T and Wan D 2013 Effect of graphene aerogel on thermal behavior of phase change materials for thermal management *Sol. Energy Mater. Sol. Cells* **113** 195–200
- [72] Harish S, Orejon D, Takata Y and Kohno M 2015 Thermal conductivity enhancement of lauric acid phase change nanocomposite with graphene nanoplatelets *Appl. Therm. Eng.* **80** 205–11
- [73] Ding P, Su S, Song N, Tang S, Liu Y and Shi L 2014 Highly thermal conductive composites with polyamide-6 covalently-grafted graphene by an in situ polymerization and thermal reduction process *Carbon* **66** 576–84
- [74] Shahil K M F and Balandin A A 2012 Graphene-multilayer graphene nanocomposites as highly efficient thermal interface materials *Nano Lett.* **12** 861–7
- [75] Kargar F, Salgado R, Legedza S, Renteria J and Balandin A A 2014 A comparative study of the thermal interface materials with graphene and boron nitride fillers *Carbon Nanotubes, Graphene, and Associated Devices VII* (9168) ed M Razeghi, Y H Lee and M Ghazinejad (International Society for Optics and Photonics, SPIE) 70–4
- [76] Ohashi M, Kawakami S, Yokogawa Y and Lai G-C 2005 Spherical aluminum nitride fillers for heat-conducting plastic packages *J. Am. Ceram. Soc.* **88** 2615–8
- [77] Lewis J S, Barani Z, Magana A S, Kargar F and Balandin A A 2019 Thermal and electrical conductivity control in hybrid composites with graphene and boron nitride fillers *Mater. Res. Express* **6** 085325
- [78] Han J, Du G, Gao W and Bai H 2019 An anisotropically high thermal conductive boron nitride/epoxy composite based on nacre-mimetic 3D network *Adv. Funct. Mater.* **29** 1900412
- [79] Yu C, Zhang J, Li Z, Tian W, Wang L, Luo J, Li Q, Fan X and Yao Y 2017 Enhanced through-plane thermal conductivity of boron nitride/epoxy composites *Composites A* **98** 25–31
- [80] Hu J, Huang Y, Yao Y, Pan G, Sun J, Zeng X, Sun R, Xu J-B, Song B and Wong C-P 2017 Polymer composite with improved thermal conductivity by constructing a hierarchically ordered three-dimensional interconnected network of BN *ACS Appl. Mater. Interfaces* **9** 13544–53 PMID: 28 362 080
- [81] Lin Z, Mcnamara A, Liu Y, Moon K S and Wong C-P 2014 Exfoliated hexagonal boron nitride-based polymer nanocomposite with enhanced thermal conductivity for electronic encapsulation *Compos. Sci. Technol.* **90** 123–8
- [82] Kim K and Kim J 2016 Vertical filler alignment of boron nitride/epoxy composite for thermal conductivity enhancement via external magnetic field *Int. J. Therm. Sci.* **100** 29–36
- [83] Yuan C, Xie B, Huang M, Wu R and Luo X 2016 Thermal conductivity enhancement of platelets aligned composites with volume fraction from 10% to 20% *Int. J. Heat Mass Transfer* **94** 20–8
- [84] Yu J, Mo H and Jiang P 2015 Polymer/boron nitride nanosheet composite with high thermal conductivity and sufficient dielectric strength *Polym. Adv. Technol.* **26** 514–20
- [85] Teng C-C, Ma C-C M, Chiou K-C and Lee T-M 2012 Synergetic effect of thermal conductive properties of epoxy composites containing functionalized multi-walled carbon nanotubes and aluminum nitride *Composites B* **43** 265–71
- [86] Zhou T, Wang X, Cheng P, Wang T, Ziong D and Wang X 2013 Improving the thermal conductivity of epoxy resin by the addition of a mixture of graphite nanoplatelets and silicon carbide microparticles *EXPRESS Polym. Lett.* **7** 585–94
- [87] Wang T *et al* 2018 Enhanced thermal conductivity of polyimide composites with boron nitride nanosheets *Sci. Rep.* **8** 1557
- [88] Sato K, Horibe H, Shirai T, Hotta Y, Nakano H, Nagai H, Mitsuishi K and Watari K 2010 Thermally conductive composite films of hexagonal boron nitride and polyimide with affinity-enhanced interfaces *J. Mater. Chem.* **20** 2749–52
- [89] Tanimoto M, Yamagata T, Miyata K and Ando S 2013 Anisotropic thermal diffusivity of hexagonal boron nitride-filled polyimide films: effects of filler particle size, aggregation, orientation, and polymer chain rigidity *ACS Appl. Mater. Interfaces* **5** 4374–82
- [90] Song H, Kim B, Kim Y, Bae Y-S, Kim J and Yoo Y 2019 Synergistic effects of various ceramic fillers on thermally conductive polyimide composite films and their model predictions *Polymers* **11** 484
- [91] Morishita T and Okamoto H 2016 Facile exfoliation and noncovalent superacid functionalization of boron nitride nanosheets and their use for highly thermally conductive and electrically insulating polymer nanocomposites *ACS Appl. Mater. Interfaces* **8** 27064–73 PMID: 27 599 203
- [92] Lee J, Jung H, Yu S, Cho S M, Tiwari V K, Velusamy D B and Park C 2016 Boron nitride nanosheets (bnss) chemically modified by ‘grafting-from’ polymerization of poly(caprolactone) for thermally conductive polymer composites *Chem. Asian J.* **11** 1921–8
- [93] Xie B-H, Huang X and Zhang G-J 2013 High thermal conductive polyvinyl alcohol composites with hexagonal boron nitride microplatelets as fillers *Compos. Sci. Technol.* **85** 98–103
- [94] Shen H, Guo J, Wang H, Zhao N and Xu J 2015 Bioinspired modification of h-BN for high thermal conductive composite films with aligned structure *ACS Appl. Mater. Interfaces* **7** 5701–8
- [95] Wang W X, Lu X, Liu J, Olorunyomi M O, Aronsson T and Shanguan D 2006 New nano-thermal interface materials (nano-TIMs) with SiC nano-particles used for heat removal in electronics packaging applications *2006 International Conf. on Electronic Materials and Packaging (Kowloon, China)* pp 1–5
- [96] Song S H, Park K H, Kim B H, Choi Y W, Jun G H, Lee D J, Kong B-S, Paik K-W and Jeon S 2013 Enhanced thermal conductivity of epoxy-graphene composites by using non-oxidized graphene flakes with non-covalent functionalization *Adv. Mater.* **25** 732–7
- [97] Yu L, Park J S, Lim Y-S, Lee C S, Shin K, Moon H J, Yang C-M, Lee Y S and Han J H 2013 Carbon hybrid fillers composed of carbon nanotubes directly grown on graphene nanoplatelets for effective thermal conductivity in epoxy composites *Nanotechnology* **24** 155604
- [98] Tian X, Itkis M E, Bekyarova E B and Haddon R C 2013 Anisotropic thermal and electrical properties of thin thermal interface layers of graphite nanoplatelet-based composites *Sci. Rep.* **3** 1710
- [99] Biercuk M J, Llaguno M C, Radosavljevic M, Hyun J K, Johnson A T and Fischer J E 2002 Carbon nanotube composites for thermal management *Appl. Phys. Lett.* **80** 2767–9
- [100] Fu Y-X, He Z-X, Mo D-C and Lu S-S 2014 Thermal conductivity enhancement of epoxy adhesive using graphene sheets as additives *Int. J. Therm. Sci.* **86** 276–83
- [101] Mai C-K, Liu J, Evans C M, Segalman R A, Chabinyc M L, Cahill D G and Bazan G C 2016 Anisotropic thermal transport in thermoelectric composites of conjugated polyelectrolytes/single-walled carbon nanotubes *Macromolecules* **49** 4957–63
- [102] Kargar F, Barani Z, Balinskiy M, Magana A S, Lewis J S and Balandin A A 2019 Dual-functional graphene composites for electromagnetic shielding and thermal management *Adv. Electron. Mater.* **5** 1800558

- [103] Renteria J, Legedza S, Salgado R, Balandin M P, Ramirez S, Saadah M, Kargar F and Balandin A A 2015 Magnetically-functionalized self-aligning graphene fillers for high-efficiency thermal management applications *Mater. Des.* **88** 214–21
- [104] Chatterjee S, Wang J W, Kuo W S, Tai N H, Salzmann C, Li W L, Hollertz R, Nüesch F A and Chu B T T 2012 Mechanical reinforcement and thermal conductivity in expanded graphene nanoplatelets reinforced epoxy composites *Chem. Phys. Lett.* **531** 6–10
- [105] Lian G, Tuan C C, Li L, Jiao S, Wang Q, Moon K S, Cui D and Wong C P 2016 Vertically aligned and interconnected graphene networks for high thermal conductivity of epoxy composites with ultralow loading *Chem. Mater.* **28** 6096–104
- [106] Prolongo S G, Moriche R, Jiménez-Suárez A, Sánchez M and Ureña A 2014 Epoxy adhesives modified with graphene for thermal interface materials *J. Adhes.* **90** 835–47
- [107] Tang B, Hu G, Gao H and Hai L 2015 Application of graphene as filler to improve thermal transport property of epoxy resin for thermal interface materials *Int. J. Heat Mass Transfer* **85** 420–9
- [108] Dmitriev A A, Dmitriev A S, Makarov P and Mikhailova I 2018 New nanocomposite surfaces and thermal interface materials based on mesoscopic microspheres, polymers and graphene flakes *AIP Conf. Proc.* **1957** 020003
- [109] Wang Y, Yu J, Dai W, Song Y, Wang D, Zeng L and Jiang N 2015 Enhanced thermal and electrical properties of epoxy composites reinforced with graphene nanoplatelets *Polym. Compos.* **36** 556–65
- [110] Moriche R, Prolongo S G, Sánchez M, Jiménez-Suárez A, Chamizo F J and Ureña A 2016 Thermal conductivity and lap shear strength of GNP/epoxy nanocomposites adhesives *Int. J. Adhes. Adhes.* **68** 407–10
- [111] Eksik O, Bartolucci S F, Gupta T, Fard H, Borca-Tasciuc T and Koratkar N 2016 A novel approach to enhance the thermal conductivity of epoxy nanocomposites using graphene core-shell additives *Carbon* **101** 239–44
- [112] Park W, Guo Y, Li X, Hu J, Liu L, Ruan X and Chen Y P 2015 High-performance thermal interface material based on few-layer graphene composite *J. Phys. Chem. C* **119** 26753–9
- [113] Shtein M, Nadiv R, Buzaglo M and Regev O 2015 Graphene-based hybrid composites for efficient thermal management of electronic devices *ACS Appl. Mater. Interfaces* **7** 23725–30
- [114] Song N, Yang J, Ding P, Tang S and Shi L 2015 Effect of polymer modifier chain length on thermal conductive property of polyamide 6/graphene nanocomposites *Composites A* **73** 232–41
- [115] Li A, Zhang C and Zhang Y-F 2017 RGO/TPU composite with a segregated structure as thermal interface material *Composites A* **101** 108–14
- [116] Gong J, Liu Z, Yu J, Dai D, Dai W, Du S, Li C, Jiang N, Zhan Z and Lin C-T 2016 Graphene woven fabric-reinforced polyimide films with enhanced and anisotropic thermal conductivity *Composites A* **87** 290–6
- [117] Song N, Jiao D, Ding P, Cui S, Tang S and Shi L 2016 Anisotropic thermally conductive flexible films based on nanofibrillated cellulose and aligned graphene nanosheets *J. Mater. Chem. C* **4** 305–14
- [118] Cui X, Ding P, Zhuang N, Shi L, Song N and Tang S 2015 Thermal conductive and mechanical properties of polymeric composites based on solution-exfoliated boron nitride and graphene nanosheets: a morphology-promoted synergistic effect *ACS Appl. Mater. Interfaces* **7** 19068–75
- [119] Fang X, Fan L W, Ding Q, Wang X, Yao X L, Hou J F, Yu Z T, Cheng G H, Hu Y C and Cen K F 2013 Increased thermal conductivity of eicosane-based composite phase change materials in the presence of graphene nanoplatelets *Energy Fuels* **27** 4041–7
- [120] Kumar P, Yadav M K, Panwar N, Kumar A and Singhal R 2019 Temperature dependent thermal conductivity of free-standing reduced graphene oxide/poly (vinylidene fluoride-co-hexafluoropropylene) composite thin film *Mater. Res. Express* **6** 115604
- [121] Barani Z, Mohammadzadeh A, Geremew A, Huang C-Y, Coleman D, Mangolini L, Kargar F and Balandin A A 2020 Thermal properties of the binary-filler hybrid composites with graphene and copper nanoparticles *Adv. Funct. Mater.* **30** 1904008
- [122] Dang T M L, Kim C-Y, Zhang Y, Yang J-F, Masaki T and Yoon D-H 2017 Enhanced thermal conductivity of polymer composites via hybrid fillers of anisotropic aluminum nitride whiskers and isotropic spheres *Composites B* **114** 237–46
- [123] Kim K, Kim M and Kim J 2014 Thermal and mechanical properties of epoxy composites with a binary particle filler system consisting of aggregated and whisker type boron nitride particles *Compos. Sci. Technol.* **103** 72–7
- [124] Sun R, Yao H, Zhang H-B, Li Y, Mai Y-W and Yu Z-Z 2016 Decoration of defect-free graphene nanoplatelets with alumina for thermally conductive and electrically insulating epoxy composites *Compos. Sci. Technol.* **137** 16–23
- [125] Wang F, Zeng X, Yao Y, Sun R, Xu J and Wong C-P 2016 Silver nanoparticle-deposited boron nitride nanosheets as fillers for polymeric composites with high thermal conductivity *Sci. Rep.* **6** 19394
- [126] Im H and Kim J 2012 Thermal conductivity of a graphene oxide-carbon nanotube hybrid/epoxy composite *Carbon* **50** 5429–40
- [127] Kim K, Ju H and Kim J 2016 Vertical particle alignment of boron nitride and silicon carbide binary filler system for thermal conductivity enhancement *Compos. Sci. Technol.* **123** 99–105
- [128] Yao Y, Sun J, Zeng X, Sun R, Xu J-B and Wong C-P 2018 Construction of 3D skeleton for polymer composites achieving a high thermal conductivity *Small* **14** 1704044
- [129] Zhou T, Wang X, Liu X and Xiong D 2010 Improved thermal conductivity of epoxy composites using a hybrid multi-walled carbon nanotube/micro-SiC filler *Carbon* **48** 1171–6
- [130] Choi S and Kim J 2013 Thermal conductivity of epoxy composites with a binary-particle system of aluminum oxide and aluminum nitride fillers *Composites B* **51** 140–7
- [131] Tang B, Li X, Huang W, Yu H and Ling X 2018 Graphene-assisted thermal interface materials with a satisfied interface contact level between the matrix and fillers *Nanoscale Res. Lett.* **13** 276
- [132] Yuan W, Xiao Q, Li L and Xu T 2016 Thermal conductivity of epoxy adhesive enhanced by hybrid graphene oxide/AlN particles *Appl. Therm. Eng.* **106** 1067–74
- [133] Ma A J, Chen W and Hou Y 2012 Enhanced thermal conductivity of epoxy composites with MWCNTs/AlN hybrid filler *Polym.-Plast. Technol. Eng.* **51** 1578–82
- [134] Zhang P, Li Q and Xuan Y M 2014 Thermal contact resistance of epoxy composites incorporated with nano-copper particles and the multi-walled carbon nanotubes *Composites A* **57** 1–7
- [135] Yang S-Y, Lin W-N, Huang Y-L, Tien H-W, Wang J-Y, Ma C-C M, Li S-M and Wang Y-S 2011 Synergetic effects of graphene platelets and carbon nanotubes on the mechanical and thermal properties of epoxy composites *Carbon* **49** 793–803
- [136] Chen L, Zhao P, Xie H and Yu W 2016 Thermal properties of epoxy resin based thermal interfacial materials by filling Ag nanoparticle-decorated graphene nanosheets *Compos. Sci. Technol.* **125** 17–21
- [137] Liu C, Chen C, Wang H, Chen M, Zhou D, Xu Z and Yu W 2019 Synergistic effect of irregular shaped particles and

- graphene on the thermal conductivity of epoxy composites *Polym. Compos.* **40** E1294–300
- [138] Du F-P, Yang W, Zhang F, Tang C-Y, Liu S-P, Yin L and Law W-C 2015 Enhancing the heat transfer efficiency in graphene-epoxy nanocomposites using a magnesium oxide-graphene hybrid structure *ACS Appl. Mater. Interfaces* **7** 14397–403 PMID: 26 075 677.
- [139] Zeng C, Lu S, Song L, Xiao X, Gao J, Pan L, He Z and Yu J 2015 Enhanced thermal properties in a hybrid graphene-alumina filler for epoxy composites *RSC Adv.* **5** 35773–82
- [140] Huang T, Zeng X, Yao Y, Sun R, Meng F, Xu J and Wong C 2016 Boron nitride@graphene oxide hybrids for epoxy composites with enhanced thermal conductivity *RSC Adv.* **6** 35847–54
- [141] Li T-L and Hsu S L-C 2010 Enhanced thermal conductivity of polyimide films via a hybrid of micro- and nano-sized boron nitride *J. Phys. Chem. B* **114** 6825–9
- [142] Zhou Y, Yu S, Niu H and Liu F 2018 Synergistic improvement in thermal conductivity of polyimide nanocomposite films using boron nitride coated copper nanoparticles and nanowires *Polymers* **10** 1412
- [143] Tsai M-H, Tseng I-H, Chiang J-C and Li J-J 2014 Flexible polyimide films hybrid with functionalized boron nitride and graphene oxide simultaneously to improve thermal conduction and dimensional stability *ACS Appl. Mater. Interfaces* **6** 8639–45
- [144] Shao L, Shi L, Li X, Song N and Ding P 2016 Synergistic effect of BN and graphene nanosheets in 3D framework on the enhancement of thermal conductive properties of polymeric composites *Compos. Sci. Technol.* **135** 83–91
- [145] Yu J, Choi H K, Kim H S and Kim S Y 2016 Synergistic effect of hybrid graphene nanoplatelet and multi-walled carbon nanotube fillers on the thermal conductivity of polymer composites and theoretical modeling of the synergistic effect *Composites A* **88** 79–85
- [146] Gu J, Guo Y, Yang X, Liang C, Geng W, Tang L, Li N and Zhang Q 2017 Synergistic improvement of thermal conductivities of polyphenylene sulfide composites filled with boron nitride hybrid fillers *Composites A* **95** 267–73
- [147] Pak S Y, Kim H M, Kim S Y and Youn J R 2012 Synergistic improvement of thermal conductivity of thermoplastic composites with mixed boron nitride and multi-walled carbon nanotube fillers *Carbon* **50** 4830–8
- [148] Zhou Y, Zhuang X, Wu F and Liu F 2018 High-performance thermal management nanocomposites: Silver functionalized graphene nanosheets and multiwalled carbon nanotube *Crystals* **8** 398
- [149] Zhao B, Wang S, Zhao C, Li R, Hamidinejad S M, Kazemi Y and Park C B 2018 Synergism between carbon materials and Ni chains in flexible poly(vinylidene fluoride) composite films with high heat dissipation to improve electromagnetic shielding properties *Carbon* **127** 469–78
- [150] Ren F, Song D, Li Z, Jia L, Zhao Y, Yan D and Ren P 2018 Synergistic effect of graphene nanosheets and carbonyl iron-nickel alloy hybrid filler on electromagnetic interference shielding and thermal conductivity of cyanate ester composites *J. Mater. Chem. C* **6** 1476–86
- [151] Jiang J, Yang S, Li L and Bai S 2020 High thermal conductivity polylactic acid composite for 3D printing: Synergistic effect of graphene and alumina *Polym. Adv. Technol.* **31** 1291–9
- [152] Balandin A A, Ghosh S, Bao W, Calizo I, Teweldebrhan D, Miao F and Lau C N 2008 Superior thermal conductivity of single-layer graphene *Nano Lett.* **8** 902–7 PMID: 18 284 217
- [153] Balandin A A 2011 Thermal properties of graphene and nanostructured carbon materials *Nat. Mater.* **10** 569–81
- [154] Ghosh S, Calizo I, Teweldebrhan D, Pokatilov E P, Nika D L, Balandin A A, Bao W, Miao F and Lau C N 2008 Extremely high thermal conductivity of graphene: Prospects for thermal management applications in nanoelectronic circuits *Appl. Phys. Lett.* **92** 151911
- [155] Seol J H *et al* 2010 Two-dimensional phonon transport in supported graphene *Science* **328** 213–6
- [156] Cai W, Moore A L, Zhu Y, Li X, Chen S, Shi L and Ruoff R S 2010 Thermal transport in suspended and supported monolayer graphene grown by chemical vapor deposition *Nano Lett.* **10** 1645–51
- [157] Wang H, Kurata K, Fukunaga T, Ago H, Takamatsu H, Zhang X, Ikuta T, Takahashi K, Nishiyama T and Takata Y 2016 Simultaneous measurement of electrical and thermal conductivities of suspended monolayer graphene *J. Appl. Phys.* **119** 244306
- [158] Zhang P, Zeng J, Zhai S, Xian Y, Yang D and Li Q 2017 Thermal properties of graphene filled polymer composite thermal interface materials *Macromol. Mater. Eng.* **302** 1700068
- [159] Li A, Zhang C and Zhang Y F 2017 Thermal conductivity of graphene-polymer composites: mechanisms, properties, and applications *Polymers* **9** 437
- [160] Balandin A A 2020 Phononics of graphene and related materials *ACS Nano* **14** 5170–8
- [161] Xie Y, Xu S, Xu Z, Wu H, Deng C and Wang X 2016 Interface-mediated extremely low thermal conductivity of graphene aerogel *Carbon* **98** 381–90
- [162] Atif R, Shyha I and Inam F 2016 Mechanical, thermal, and electrical properties of graphene-epoxy nanocomposites—a review *Polymers* **8** 281
- [163] Hernandez Y *et al* 2008 High-yield production of graphene by liquid-phase exfoliation of graphite *Nat. Nanotechnol.* **3** 563–8
- [164] Lotya M *et al* 2009 Liquid phase production of graphene by exfoliation of graphite in surfactant/water solutions *JACS* **131** 3611–20
- [165] Coleman J N *et al* 2011 Two-dimensional nanosheets produced by liquid exfoliation of layered materials *Science* **331** 568–71
- [166] Nicolosi V, Chhowalla M, Kanatzidis M G, Strano M S and Coleman J N 2013 Liquid exfoliation of layered materials *Science* **340** 1226419
- [167] Yu P, Lowe S E, Simon G P and Zhong Y L 2015 Electrochemical exfoliation of graphite and production of functional graphene *Curr. Opin. Colloid Interface Sci.* **20** 329–38
- [168] Hummers W S and Offeman R E 1958 Preparation of graphitic oxide *JACS* **80** 1339
- [169] Stankovich S, Dikin D A, Dommett G H B, Kohlhaas K M, Zimney E J, Stach E A, Piner R D, Nguyen S B T and Ruoff R S 2006 Graphene-based composite materials *Nature* **442** 282–6
- [170] Stankovich S, Dikin D A, Piner R D, Kohlhaas K A, Kleinhammes A, Jia Y, Wu Y, Nguyen S B T and Ruoff R S 2007 Synthesis of graphene-based nanosheets via chemical reduction of exfoliated graphite oxide *Carbon* **45** 1558–65
- [171] Nethravathi C and Rajamathi M 2008 Chemically modified graphene sheets produced by the solvothermal reduction of colloidal dispersions of graphite oxide *Carbon* **46** 1994–8
- [172] Chen J, Yao B, Li C and Shi G 2013 An improved Hummers method for eco-friendly synthesis of graphene oxide *Carbon* **64** 225–9
- [173] Zaaba N I, Foo K L, Hashim U, Tan S J, Liu W-W and Voon C H 2017 Synthesis of graphene oxide using modified Hummers method: solvent influence *Procedia Eng.* **184** 469–77
- [174] Nagyte V *et al* 2020 Raman fingerprints of graphene produced by anodic electrochemical exfoliation *Nano Lett.* **20** 3411–3419
- [175] Eigler S, Dotzer C and Hirsch A 2012 Visualization of defect densities in reduced graphene oxide *Carbon* **50** 3666–73

- [176] Chen J-H, Cullen W G, Jang C, Fuhrer M S and Williams E D 2009 Defect scattering in graphene *Phys. Rev. Lett.* **102** 236805
- [177] Hao F, Fang D and Xu Z 2011 Mechanical and thermal transport properties of graphene with defects *Appl. Phys. Lett.* **99** 041901
- [178] Mortazavi B and Ahzi S 2013 Thermal conductivity and tensile response of defective graphene: a molecular dynamics study *Carbon* **63** 460–70
- [179] Malekpour H, Ramnani P, Srinivasan S, Balasubramanian G, Nika D L, Mulchandani A, Lake R K and Balandin A A 2016 Thermal conductivity of graphene with defects induced by electron beam irradiation *Nanoscale* **8** 14608–16
- [180] Zhang Y Y, Cheng Y, Pei Q X, Wang C M and Xiang Y 2012 Thermal conductivity of defective graphene *Phys. Lett. A* **376** 3668–72
- [181] Paton K R *et al* 2014 Scalable production of large quantities of defect-free few-layer graphene by shear exfoliation in liquids *Nat. Mater.* **13** 624–30
- [182] Nika D L, Pokatilov E P, Askerov A S and Balandin A A 2009 Phonon thermal conduction in graphene: role of Umklapp and edge roughness scattering *Phys. Rev. B* **79** 155413
- [183] Nika D L, Ghosh S, Pokatilov E P and Balandin A A 2009 Lattice thermal conductivity of graphene flakes: comparison with bulk graphite *Appl. Phys. Lett.* **94** 203103
- [184] Nika D L, Askerov A S and Balandin A A 2012 Anomalous size dependence of the thermal conductivity of graphene ribbons *Nano Lett.* **12** 3238–44
- [185] Zhang Z, Hu S, Chen J and Li B 2017 Hexagonal boron nitride: a promising substrate for graphene with high heat dissipation *Nanotechnology* **28** 225704
- [186] Jang W, Chen Z, Bao W, Lau C N and Dames C 2010 Thickness-dependent thermal conductivity of encased graphene and ultrathin graphite *Nano Lett.* **10** 3909–13
- [187] Pettes M T, Jo I, Yao Z and Shi L 2011 Influence of polymeric residue on the thermal conductivity of suspended bilayer graphene *Nano Lett.* **11** 1195–200
- [188] Sadeghi M M, Jo I and Shi L 2013 Phonon-interface scattering in multilayer graphene on an amorphous support *Proc. Natl Acad. Sci.* **110** 16321–6
- [189] Renteria J, Nika D and Balandin A 2014 Graphene thermal properties: applications in thermal management and energy storage *Appl. Sci.* **4** 525–47
- [190] Sun Y, Tang B, Huang W, Wang S, Wang Z, Wang X, Zhu Y and Tao C 2016 Preparation of graphene modified epoxy resin with high thermal conductivity by optimizing the morphology of filler *Appl. Therm. Eng.* **103** 892–900
- [191] Shen X, Wang Z, Wu Y, Liu X, He Y B and Kim J K 2016 Multilayer graphene enables higher efficiency in improving thermal conductivities of graphene/epoxy composites *Nano Lett.* **16** 3585–93
- [192] Correa G C, Foss C J and Aksamija Z 2017 Interface thermal conductance of van der Waals monolayers on amorphous substrates *Nanotechnology* **28** 135402
- [193] Chen J, Walther J H and Koumoutsakos P 2015 Covalently bonded graphene-carbon nanotube hybrid for high-performance thermal interfaces *Adv. Funct. Mater.* **25** 7539–45
- [194] Chu K, Li W S and Tang F L 2013 Flatness-dependent thermal conductivity of graphene-based composites *Phys. Lett. A* **377** 910–4
- [195] Li H, Ying H, Chen X, Nika D L, Cocemasov A I, Cai W, Balandin A A and Chen S 2014 Thermal conductivity of twisted bilayer graphene *Nanoscale* **6** 13402–8
- [196] Schueler R, Petermann J, Schulte K and Wentzel H-P 1997 Agglomeration and electrical percolation behavior of carbon black dispersed in epoxy resin *J. Appl. Polym. Sci.* **63** 1741–6
- [197] Sandler J K W, Kirk J E, Kinloch I A, Shaffer M S P and Windle A H 2003 Ultra-low electrical percolation threshold in carbon-nanotube-epoxy composites *Polymer* **44** 5893–9 In Honour of Ian Ward's 75th Birthday
- [198] Gelves G A, Sundararaj U and Haber J A 2005 Electrostatically dissipative polystyrene nanocomposites containing copper nanowires *Macromol. Rapid Commun.* **26** 1677–81
- [199] Bauhofer W and Kovacs J Z 2009 A review and analysis of electrical percolation in carbon nanotube polymer composites *Compos. Sci. Technol.* **69** 1486–98
- [200] White S I, Mutiso R M, Vora P M, Jahnke D, Hsu S, Kikkawa J M, Li J, Fischer J E and Winey K I 2010 Electrical percolation behavior in silver nanowire-polystyrene composites: simulation and experiment *Adv. Funct. Mater.* **20** 2709–16
- [201] Cui W, Du F, Zhao J, Zhang W, Yang Y, Xie X and Mai Y-W 2011 Improving thermal conductivity while retaining high electrical resistivity of epoxy composites by incorporating silica-coated multi-walled carbon nanotubes *Carbon* **49** 495–500
- [202] Liang Q, Yao X, Wang W, Liu Y and Wong C P 2011 A three-dimensional vertically aligned functionalized multilayer graphene architecture: an approach for graphene-based thermal interfacial materials *ACS Nano* **5** 2392–401
- [203] Fukushima H, Drzal L T, Rook B P and Rich M J 2006 Thermal conductivity of exfoliated graphite nanocomposites *J. Therm. Anal. Calorim.* **85** 235–8
- [204] Nan C-W, Birringer R, Clarke D R and Gleiter H 1997 Effective thermal conductivity of particulate composites with interfacial thermal resistance *J. Appl. Phys.* **81** 6692–9
- [205] Xie S H, Liu Y Y and Li J Y 2008 Comparison of the effective conductivity between composites reinforced by graphene nanosheets and carbon nanotubes *Appl. Phys. Lett.* **92** 243121
- [206] Lin S and Buehler M J 2013 The effect of non-covalent functionalization on the thermal conductance of graphene/organic interfaces *Nanotechnology* **24** 165702
- [207] Rohini R, Katti P and Bose S 2015 Tailoring the interface in graphene/thermoset polymer composites: a critical review *Polymer* **70** A17–34
- [208] Vasiraju V, Norris D and Vaddiraju S 2017 Thermal transport through Zn₃P₂ nanowire-BN microparticle/nanoparticle composites and hybrids *Mater. Res. Express* **4** 075041
- [209] Speranza G 2019 The role of functionalization in the applications of carbon materials: an overview *C—Journal of Carbon Research* **5** 84
- [210] Wang M, Galpaya D, Lai Z B, Xu Y and Yan C 2014 Surface functionalization on the thermal conductivity of graphene-polymer nanocomposites *Int. J. Smart Nano Mater.* **5** 123–32
- [211] Alexeev D, Chen J, Walther J H, Giapis K P, Angelikopoulos P and Koumoutsakos P 2015 Kapitza resistance between few-layer graphene and water: liquid layering effects *Nano Lett.* **15** 5744–9
- [212] Wang Y, Zhan H F, Xiang Y, Yang C, Wang C M and Zhang Y Y 2015 Effect of covalent functionalization on thermal transport across graphene-polymer interfaces *J. Phys. Chem. C* **119** 12731–8
- [213] Wang Y, Yang C, Mai Y-W and Zhang Y 2016 Effect of non-covalent functionalisation on thermal and mechanical properties of graphene-polymer nanocomposites *Carbon* **102** 311–8
- [214] Liu X, Zhang G and Zhang Y W 2014 Thermal conduction across graphene cross-linkers *J. Phys. Chem. C* **118** 12541–7
- [215] Zabihi Z and Araghi H 2016 Effect of functional groups on thermal conductivity of graphene/paraffin nanocomposite *Phys. Lett. A* **380** 3828–31

- [216] Shen X, Wang Z, Wu Y, Liu X and Kim J-K 2016 Effect of functionalization on thermal conductivities of graphene/epoxy composites *Carbon* **108** 412–22
- [217] Cao L, Liu X, Na H, Wu Y, Zheng W and Zhu J 2013 How a bio-based epoxy monomer enhanced the properties of diglycidyl ether of bisphenol a (dgeba)/graphene composites *J. Mater. Chem. A* **1** 5081–8
- [218] Huang J, Zhu Y, Xu L, Chen J, Jiang W and Nie X 2016 Massive enhancement in the thermal conductivity of polymer composites by trapping graphene at the interface of a polymer blend *Compos. Sci. Technol.* **129** 160–5
- [219] An F, Li X, Min P, Liu P, Jiang Z-G and Yu Z-Z 2018 Vertically aligned high-quality graphene foams for anisotropically conductive polymer composites with ultrahigh through-plane thermal conductivities *ACS Appl. Mater. Interfaces* **10** 17383–92
- [220] Li X-H, Liu P, Li X, An F, Min P, Liao K-N and Yu Z-Z 2018 Vertically aligned, ultralight and highly compressive all-graphitized graphene aerogels for highly thermally conductive polymer composites *Carbon* **140** 624–33
- [221] Liang X and Dai F 2019 Epoxy nanocomposites with reduced graphene oxide-constructed three-dimensional networks of single wall carbon nanotube for enhanced thermal management capability with low filler loading *ACS Appl. Mater. Interfaces* **12** 3051–8
- [222] Bo Z, Zhu H, Ying C, Yang H, Wu S, Kong J, Yang S, Wei X, Yan J and Cen K 2019 Tree-inspired radially aligned, bimodal graphene frameworks for highly efficient and isotropic thermal transport *Nanoscale* **11** 21249–58
- [223] Wang Z, Cao Y, Pan D and Hu S 2020 Vertically aligned and interconnected graphite and graphene oxide networks leading to enhanced thermal conductivity of polymer composites *Polymers* **12** 1121
- [224] Liu Z *et al* 2019 Graphene foam-embedded epoxy composites with significant thermal conductivity enhancement *Nanoscale* **11** 17600–6
- [225] Song S, Wang J, Liu C, Wang J and Zhang Y 2019 A facile route to fabricate thermally conductive and electrically insulating polymer composites with 3D interconnected graphene at an ultralow filler loading *Nanoscale* **11** 15234–44
- [226] Kumar P, Yu S, Shahzad F, Hong S M, Kim Y-H and Koo C M 2016 Ultrahigh electrically and thermally conductive self-aligned graphene/polymer composites using large-area reduced graphene oxides *Carbon* **101** 120–8
- [227] Kim H S, Bae H S, Yu J and Kim S Y 2016 Thermal conductivity of polymer composites with the geometrical characteristics of graphene nanoplatelets *Sci. Rep.* **6** 1–9
- [228] Zhu H, Li Y, Fang Z, Xu J, Cao F, Wan J, Preston C, Yang B and Hu L 2014 Highly thermally conductive papers with percolative layered boron nitride nanosheets *ACS Nano* **8** 3606–13
- [229] Luo F, Wu K, Guo H, Zhao Q and Lu M 2016 Anisotropic thermal conductivity and flame retardancy of nanocomposite based on mesogenic epoxy and reduced graphene oxide bulk *Compos. Sci. Technol.* **132** 1–8
- [230] Yao Y, Zeng X, Sun R, Xu J-B and Wong C-P 2016 Highly thermally conductive composite papers prepared based on the thought of bioinspired engineering *ACS Appl. Mater. Interfaces* **8** 15645–53 PMID: 27 253 387
- [231] Song N, Hou X, Chen L, Cui S, Shi L and Ding P 2017 A green plastic constructed from cellulose and functionalized graphene with high thermal conductivity *ACS Appl. Mater. Interfaces* **9** 17914–22 PMID: 28 467 836
- [232] Li G, Tian X, Xu X, Zhou C, Wu J, Li Q, Zhang L, Yang F and Li Y 2017 Fabrication of robust and highly thermally conductive nanofibrillated cellulose/graphite nanoplatelets composite papers *Compos. Sci. Technol.* **138** 179–85
- [233] Han M, Xie Y, Liu J, Zhang J and Wang X 2018 Significantly reduced c-axis thermal diffusivity of graphene-based papers *Nanotechnology* **29** 265702
- [234] Yuan G-J, Xie J-F, Li H-H, Shan B, Zhang X-X, Liu J, Li L and Tian Y-Z 2020 Thermally reduced graphene oxide/carbon nanotube composite films for thermal packaging applications *Materials* **13** 317
- [235] Xu X *et al* 2014 Length-dependent thermal conductivity in suspended single-layer graphene *Nat. Commun.* **5** 1–6
- [236] Liu Y, Hu C, Huang J, Sumpter B G and Qiao R 2015 Tuning interfacial thermal conductance of graphene embedded in soft materials by vacancy defects *J. Chem. Phys.* **142** 244703
- [237] Wang Y, Yang C, Cheng Y and Zhang Y 2015 A molecular dynamics study on thermal and mechanical properties of graphene-paraffin nanocomposites *RSC Adv.* **5** 82638–44
- [238] Peng S, Fuchs A and Wirtz R A 2004 Polymeric phase change composites for thermal energy storage *J. Appl. Polym. Sci.* **93** 1240–51
- [239] Martin C A, Sandler J K W, Shaffer M S P, Schwarz M-K, Bauhofer W, Schulte K and Windle A H 2004 Formation of percolating networks in multi-wall carbon-nanotube-epoxy composites *Compos. Sci. Technol.* **64** 2309–16
- [240] Pang H, Chen T, Zhang G, Zeng B and Li Z-M 2010 An electrically conducting polymer/graphene composite with a very low percolation threshold *Mater. Lett.* **64** 2226–9
- [241] Zhang H-B, Zheng W-G, Yan Q, Yang Y, Wang J-W, Lu Z-H, Ji G-Y and Yu Z-Z 2010 Electrically conductive polyethylene terephthalate/graphene nanocomposites prepared by melt compounding *Polymer* **51** 1191–6
- [242] Potts J R, Dreyer D R, Bielawski C W and Ruoff R S 2011 Graphene-based polymer nanocomposites *Polymer* **52** 5–25
- [243] Bujard P 1988 Thermal conductivity of boron nitride filled epoxy resins: temperature dependence and influence of sample preparation *InterSociety Conf. on Thermal Phenomena in the Fabrication and Operation of Electronic Components. I-THERM '88 (Los Angeles, CA)* pp 41–9
- [244] Shenogina N, Shenogin S, Xue L and Keblinski P 2005 On the lack of thermal percolation in carbon nanotube composites *Appl. Phys. Lett.* **87** 133106
- [245] Ding Y, Alias H, Wen D and Williams R A 2006 Heat transfer of aqueous suspensions of carbon nanotubes (CNT nanofluids) *Int. J. Heat Mass Transfer* **49** 240–50
- [246] Bonnet P, Sireude D, Garnier B and Chauvet O 2007 Thermal properties and percolation in carbon nanotube-polymer composites *Appl. Phys. Lett.* **91** 201910
- [247] Zheng R, Gao J, Wang J, Feng S P, Ohtani H, Wang J and Chen G 2012 Thermal percolation in stable graphite suspensions *Nano Lett.* **12** 188–92
- [248] Gu J, Xie C, Li H, Dang J, Geng W and Zhang Q 2014 Thermal percolation behavior of graphene nanoplatelets/polyphenylene sulfide thermal conductivity composites *Polym. Compos.* **35** 1087–92
- [249] Shtein M, Nadiv R, Buzaglo M, Kahil K and Regev O 2015 Thermally conductive graphene-polymer composites: size, percolation, and synergy effects *Chem. Mater.* **27** 2100–6
- [250] Zhang G, Xia Y, Wang H, Tao Y, Tao G, Tu S and Wu H 2010 A percolation model of thermal conductivity for filled polymer composites *J. Compos. Mater.* **44** 963–70
- [251] Wattanakul K, Manuspiya H and Yanumet N 2011 Thermal conductivity and mechanical properties of BN-filled epoxy composite: effects of filler content, mixing conditions, and BN agglomerate size *J. Compos. Mater.* **45** 1967–80
- [252] Kim B-W, Pfeifer S, Park S-H and Bandaru P R 2011 The experimental determination of the onset of electrical and thermal conductivity percolation thresholds in carbon nanotube-polymer composites *MRS Proc.* 1312mrsf10-1312-ii07-06

- [253] Garnett J C M and Larmor J 1906 VII. colours in metal glasses, in metallic films, and in metallic solutions *Philosophical Transactions of the Royal Society of London. Series A, Containing Papers of a Mathematical or Physical Character* **205** 237–88
- [254] Nielsen L E 1973 Thermal conductivity of particulate-filled polymers *J. Appl. Polym. Sci.* **17** 3819–20
- [255] Nielsen L E 1974 The thermal and electrical conductivity of two-phase systems *Ind. Eng. Chem. Fundam.* **13** 17–20
- [256] Agari Y and Uno T 1986 Estimation on thermal conductivities of filled polymers *J. Appl. Polym. Sci.* **32** 5705–12
- [257] Devpura A, Phelan P E and Prasher R S 2000 Percolation theory applied to the analysis of thermal interface materials in flip-chip technology *ITHERM 2000. The Seventh Intersociety Conf. on Thermal and Thermomechanical Phenomena in Electronic Systems (Cat. No.00CH37069)* pp 21–8
- [258] Nan C-W, Liu G, Lin Y and Li M 2004 Interface effect on thermal conductivity of carbon nanotube composites *Appl. Phys. Lett.* **85** 3549–51
- [259] Pietrak K and Wiśniewski T S 2014 A review of models for effective thermal conductivity of composite materials *J. Power Technol.* **95** 14–24
- [260] Sichel E K, Miller R E, Abrahams M S and Buiocchi C J 1976 Heat capacity and thermal conductivity of hexagonal pyrolytic boron nitride *Phys. Rev. B* **13** 4607–11
- [261] Sevik C, Kinaci A, Haskins J B and Çağın T 2011 Characterization of thermal transport in low-dimensional boron nitride nanostructures *Phys. Rev. B* **84** 085409
- [262] Lindsay L and Broido D A 2012 Theory of thermal transport in multilayer hexagonal boron nitride and nanotubes *Phys. Rev. B* **85** 035436
- [263] Sevik C, Kinaci A, Haskins J B and Çağın T 2012 Influence of disorder on thermal transport properties of boron nitride nanostructures *Phys. Rev. B* **86** 075403
- [264] Jo I, Pettes M T, Kim J, Watanabe K, Taniguchi T, Yao Z and Shi L 2013 Thermal conductivity and phonon transport in suspended few-layer hexagonal boron nitride *Nano Lett.* **13** 550–4
- [265] Zhou H *et al* 2014 High thermal conductivity of suspended few-layer hexagonal boron nitride sheets *Nano Res.* **7** 1232–40
- [266] Wang C, Guo J, Dong L, Aiyiti A, Xu X and Li B 2016 Superior thermal conductivity in suspended bilayer hexagonal boron nitride *Sci. Rep.* **6** 1–6
- [267] Hopkins P E, Baraket M, Barnat E V, Beechem T E, Kearney S P, Duda J C, Robinson J T and Walton S G 2012 Manipulating thermal conductance at metal-graphene contacts via chemical functionalization *Nano Lett.* **12** 590–5
- [268] Foley B M, Hernández S C, Duda J C, Robinson J T, Walton S G and Hopkins P E 2015 Modifying surface energy of graphene via plasma-based chemical functionalization to tune thermal and electrical transport at metal interfaces *Nano Lett.* **15** 4876–82
- [269] Walton S G, Foley B M, Hernández S C, Boris D R, Baraket M, Duda J C, Robinson J T and Hopkins P E 2017 Plasma-based chemical functionalization of graphene to control the thermal transport at graphene-metal interfaces *Surf. Coat. Technol.* **314** 148–54
- [270] Drozdov A D and deClaville Christiansen J 2019 Thermal conductivity of highly filled polymer nanocomposites *Compos. Sci. Technol.* **182** 107717
- [271] Bar-Cohen A, Matin K and Narumanchi S 2015 Nanothermal interface materials: technology review and recent results *J. Electron. Packag.* **137** 040803
- [272] Hansson J, Zandén C, Ye L and Liu J 2016 Review of current progress of thermal interface materials for electronics thermal management applications 2016 *IEEE 16th International Conf. on Nanotechnology (IEEE-NANO)* pp 371–4
- [273] Ma T, Zhao Y, Ruan K, Liu X, Zhang J, Guo Y, Yang X, Kong J and Gu J 2019 Highly thermal conductivities, excellent mechanical robustness and flexibility, and outstanding thermal stabilities of aramid nanofiber composite papers with nacre-mimetic layered structures *ACS Appl. Mater. Interfaces* **12** 1677–86
- [274] Hou X, Chen Y, Lv L, Dai W, Zhao S, Wang Z, Fu L, Lin C-T, Jiang N and Yu J 2019 High-thermal-transport-channel construction within flexible composites via the welding of boron nitride nanosheets *ACS Appl. Nano Mater.* **2** 360–8
- [275] Prasher Ravi S., Shipley Jim, Prstic Suzana, Koning Paul and Wang Jin-lin 2003 Thermal resistance of particle laden polymeric thermal interface materials *Journal of Heat Transfer* **125** (6) 1170–77
- [276] Zhang L, Ruesch M, Zhang X, Bai Z and Liu L 2015 Tuning thermal conductivity of crystalline polymer nanofibers by interchain hydrogen bonding *RSC Adv.* **5** 87981–6
- [277] Mu L, Ji T, Chen L, Mehra N, Shi Y and Zhu J 2016 Paving the thermal highway with self-organized nanocrystals in transparent polymer composites *ACS Appl. Mater. Interfaces* **8** 29080–7
- [278] Evans W, Prasher R, Fish J, Meakin P, Phelan P and Keblinski P 2008 Effect of aggregation and interfacial thermal resistance on thermal conductivity of nanocomposites and colloidal nanofluids *Int. J. Heat Mass Transfer* **51** 1431–8
- [279] Brinkworth B J, Cross B M, Marshall R H and Yang H 1997 Thermal regulation of photovoltaic cladding *Sol. Energy* **61** 169–78
- [280] Radziemska E 2003 The effect of temperature on the power drop in crystalline silicon solar cells *Renewable Energy* **28** 1–12
- [281] Lammert M D and Schwartz R J 1977 The interdigitated back contact solar cell: a silicon solar cell for use in concentrated sunlight *IEEE Trans. Electron Devices* **24** 337–42
- [282] Han X, Wang Y and Zhu L 2011 Electrical and thermal performance of silicon concentrator solar cells immersed in dielectric liquids *Appl. Energy* **88** 4481–9
- [283] Wang Q, Gao W and Xie Z 2003 Highly thermally conductive room-temperature-vulcanized silicone rubber and silicone grease *J. Appl. Polym. Sci.* **89** 2397–9
- [284] Yu A, Ramesh P, Sun X, Bekyarova E, Itkis M E and Haddon R C 2008 Enhanced thermal conductivity in a hybrid graphite nanoplatelet–carbon nanotube filler for epoxy composites *Adv. Mater.* **20** 4740–4
- [285] Kemaloglu S, Ozkoc G and Aytac A 2010 Properties of thermally conductive micro and nano size boron nitride reinforced silicon rubber composites *Thermochim. Acta* **499** 40–7
- [286] Yang K and Gu M 2010 Enhanced thermal conductivity of epoxy nanocomposites filled with hybrid filler system of triethylenetetramine-functionalized multi-walled carbon nanotube/silane-modified nano-sized silicon carbide *Composites A* **41** 215–21
- [287] Liu C, Chen M, Zhou D, Wu D and Yu W 2017 Effect of filler shape on the thermal conductivity of thermal functional composites *J. Nanomater.* **2017** 1–15
- [288] Wang Z-G, Gong F, Yu W-C, Huang Y-F, Zhu L, Lei J, Xu J-Z and Li Z-M 2018 Synergetic enhancement of thermal conductivity by constructing hybrid conductive network in the segregated polymer composites *Compos. Sci. Technol.* **162** 7–13
- [289] Dmitriev A S 2020 Hybrid graphene nanocomposites: Thermal interface materials and functional energy materials *Graphene Production and Application* ed S Ameen *et al* (London: IntechOpen) 6 (<https://doi.org/10.5772/intechopen.89631>)
- [290] Gao Z and Zhao L 2015 Effect of nano-fillers on the thermal conductivity of epoxy composites with micro-Al₂O₃ particles *Mater. Des. (1980-2015)* **66** 176–82
- [291] Zhang L, Zhu W, Huang Y and Qi S 2019 Synergetic effects of silver nanowires and graphene oxide on thermal conductivity of epoxy composites *Nanomaterials* **9** 1264

- [292] Ferrari A C *et al* 2006 Raman spectrum of graphene and graphene layers *Phys. Rev. Lett.* **97** 187401
- [293] Ferrari A C 2007 Raman spectroscopy of graphene and graphite: Disorder, electron-phonon coupling, doping and nonadiabatic effects *Solid State Commun.* **143** 47–57
- [294] Calizo I, Bao W, Miao F, Lau C N and Balandin A A 2007 The effect of substrates on the Raman spectrum of graphene: Graphene-on-sapphire and graphene-on-glass *Appl. Phys. Lett.* **91** 201904
- [295] Cai Q, Scullion D, Falin A, Watanabe K, Taniguchi T, Chen Y, Santos E J G and Li L H 2017 Raman signature and phonon dispersion of atomically thin boron nitride *Nanoscale* **9** 3059–67
- [296] Parker W J, Jenkins R J, Butler C P and Abbott G L 1961 Flash method of determining thermal diffusivity, heat capacity, and thermal conductivity *J. Appl. Phys.* **32** 1679–84
- [297] Gaal P S, Thermitus M A and Stroe D E 2004 Thermal conductivity measurements using the flash method *J. Therm. Anal. Calorim.* **78** 185–9
- [298] Dworkin A S, Sasmor D J and Van Artsdalen E R 1954 The thermodynamics of boron nitride; low-temperature heat capacity and entropy; heats of combustion and formation *J. Chem. Phys.* **22** 837–42
- [299] Butland A T D and Maddison R J 1973 The specific heat of graphite: an evaluation of measurements *J. Nucl. Mater.* **49** 45–56
- [300] Hone J 2001 Phonons and thermal properties of carbon nanotubes *Carbon Nanotubes: Synthesis, Structure, Properties, and Applications* ed M S Dresselhaus *et al* 80 (Berlin: Springer) (https://doi.org/10.1007/3-540-39947-X_11)
- [301] Nika D L, Cocemasov A I and Balandin A A 2014 Specific heat of twisted bilayer graphene: engineering phonons by atomic plane rotations *Appl. Phys. Lett.* **105** 031904
- [302] Cocemasov A I, Nika D L and Balandin A A 2015 Engineering of the thermodynamic properties of bilayer graphene by atomic plane rotations: the role of the out-of-plane phonons *Nanoscale* **7** 12851–9
- [303] Sandler J, Shaffer M S P, Prasse T, Bauhofer W, Schulte K and Windle A H 1999 Development of a dispersion process for carbon nanotubes in an epoxy matrix and the resulting electrical properties *Polymer* **40** 5967–71
- [304] Wang Q, Dai J, Li W, Wei Z and Jiang J 2008 The effects of CNT alignment on electrical conductivity and mechanical properties of SWNT/epoxy nanocomposites *Compos. Sci. Technol.* **68** 1644–8
- [305] Yu W, Xie H, Yin L, Zhao J, Xia L and Chen L 2015 Exceptionally high thermal conductivity of thermal grease: Synergistic effects of graphene and alumina *Int. J. Therm. Sci.* **91** 76–82
- [306] Cumberland D J, Crawford R J and Sprevak D 1989 A statistical model for the random packing of real powder particles *European Polymer Journal* **25** 1173 - 1182
- [307] Guan F-L, Gui C-X, Zhang H-B, Jiang Z-G, Jiang Y and Yu Z-Z 2016 Enhanced thermal conductivity and satisfactory flame retardancy of epoxy/alumina composites by combination with graphene nanoplatelets and magnesium hydroxide *Composites B* **98** 134–40
- [308] Liu M-S, Lin M C-C, Huang I-T and Wang C-C 2006 Enhancement of thermal conductivity with CuO for nanofluids *Chem. Eng. Technol.* **29** 72–7
- [309] Gupta A, Liu Y, Zamora N and Paddock T 2006 Thermal imaging for detecting thermal interface issues in assembly and reliability stressing *Thermal and Thermomechanical Proc. 10th Intersociety Conf. on Phenomena in Electronics Systems, 2006. IThERM 2006* 945
- [310] Due J and Robinson A J 2013 Reliability of thermal interface materials: a review *Appl. Therm. Eng.* **50** 455–63
- [311] Li M, Liu J, Pan S, Zhang J, Liu Y, Liu J and Lu H 2020 Highly oriented graphite aerogel fabricated by confined liquid-phase expansion for anisotropically thermally conductive epoxy composites *ACS Appl. Mater. Interfaces* **12** 27476–84
- [312] Luo X, Xu Y and Chung D D L 2000 Thermal stability of thermal interface pastes, evaluated by thermal contact conductance measurement *J. Electron. Packag.* **123** 309–11
- [313] Dal S L B 2004 Degradation mechanisms of siloxane-based thermal interface materials under reliability stress conditions *2004 IEEE International Reliability Physics Symposium. Proc.* pp 537–42
- [314] Ramaswamy C, Shinde S, Pompeo F, Sablinski W and Bradley S 2004 Phase change materials as a viable thermal interface material for high-power electronic applications *The Ninth Intersociety Conf. on Thermal and Thermomechanical Phenomena In Electronic Systems (IEEE Cat. No.04CH37543)* vol 2, pp 687–91
- [315] Bharatham L, Fong W S, Torresola J and Koang C C 2005 Qualification of phase change thermal interface material for wave solder heat sink on FCBGA package *2005 7th Electronic Packaging Technology Conf. vol 2 (Singapore)*
- [316] Gowda A, Esler D, Paisner S N, Tonapi S, Nagarkar K and Srihari K 2005 Reliability testing of silicone-based thermal greases [IC cooling applications] *Semiconductor Thermal Measurement and Management IEEE Twenty First Annual IEEE Symposium, 2005* pp 64–71
- [317] Khuu V, Osterman M, Bar-Cohen A and Pecht M 2009 Effects of temperature cycling and elevated temperature/humidity on the thermal performance of thermal interface materials *IEEE Trans. Device Mater. Reliab.* **9** 379–91
- [318] Chen C I, Ni C Y, Pan H Y, Chang C M and Liu D S 2009 Practical evaluation for long-term stability of thermal interface material *Exp. Tech.* **33** 28–32
- [319] Paisner S N, Touzelbaev M, Refai-Ahmed G and Yang Y 2010 New developments for a no-pump-out high-performance thermal grease *2010 12th IEEE Intersociety Conf. on Thermal and Thermomechanical Phenomena in Electronic Systems* pp 1–4
- [320] Goel N *et al* 2008 Technical review of characterization methods for thermal interface materials (TIM) *2008 11th Intersociety Conf. on Thermal and Thermomechanical Phenomena in Electronic Systems* pp 248–58
- [321] Gowda A, Zhong A, Esler D, David J, Sandeep T, Srihari K and Schattenmann F 2003 Design of a high reliability and low thermal resistance interface material for microelectronics *Proc. of the 5th Electronics Packaging Technology Conf. (EPTC 2003) (Singapore)* pp 557–62
- [322] Lewis J S, Perrier T, Mohammadzadeh A, Kargar F and Balandin A A 2020 Power cycling and reliability testing of epoxy-based graphene thermal interface materials C— *Journal of Carbon Research* **6** 26
- [323] Krehling R P and Kline D E 1969 Thermal conductivity, specific heat, and dynamic mechanical behavior of diglycidyl ether of bisphenol a cured with m-phenylenediamine *J. Appl. Polym. Sci.* **13** 2411–25
- [324] dos Santos W N, de Sousa J A and Gregorio R 2013 Thermal conductivity behaviour of polymers around glass transition and crystalline melting temperatures *Polym. Test.* **32** 987–94
- [325] Yasmin A and Daniel I M 2004 Mechanical and thermal properties of graphite platelet/epoxy composites *Polymer* **45** 8211–9
- [326] Ramanathan T *et al* 2008 Functionalized graphene sheets for polymer nanocomposites *Nat. Nanotechnol.* **3** 327–31
- [327] Bjorneklett A, Tuhus T, Halbo L and Kristiansen H 1993 Thermal resistance, thermomechanical stress and thermal cycling endurance of silicon chips bonded with adhesives *Ninth Annual IEEE Semiconductor Thermal Measurement and Management Symposium* pp 136–43